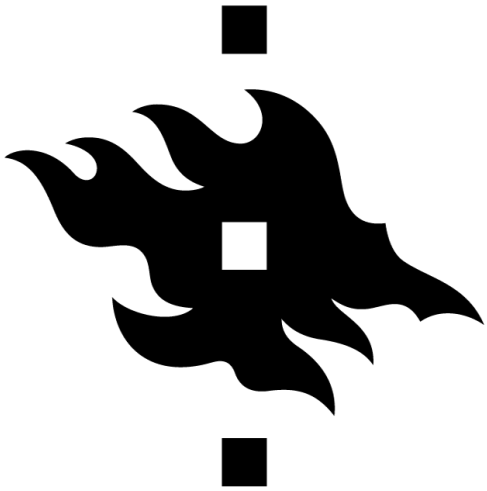

Detection thresholds of light increments and decrements

Master's Thesis

Samu Tienhaara

University of Helsinki

Faculty of Biological and Environmental Sciences

Master's Programme in Neuroscience

May 2021

HELSINGIN YLIOPISTO
HELSINGFORS UNIVERSITET
UNIVERSITY OF HELSINKI

Abstract

Faculty: Faculty of Biological and Environmental Sciences

Degree programme: Master's Programme in Neuroscience

Study track: Neuroscience

Author: Samu Tienhaara

Title: Detection thresholds of light increments and decrements

Level: Master's thesis

Month and year: 05 / 2021

Number of pages: 53

Keywords: *Human vision, Psychophysics, Visual threshold, Detection threshold, Retina, Increment, Decrement, Fullfield*

Supervisor or supervisors: Markku Kilpeläinen & Petri Ala-Laurila

Where deposited: HELDA – Digital Repository of the University of Helsinki

Additional information:

Abstract:

In visual detection, thresholds for light increments are higher than thresholds for light decrements. This asymmetry has been often ascribed to the differential processing of ON and OFF pathways in the retina, as ON and OFF retinal ganglion cells have been found to respond to increments and decrements, respectively.

In this study, the performance of human participants in detecting spatially restricted (diameter 1.17 degrees of visual angle) and unrestricted increments and decrements was measured using a two-interval forced choice task. Background light intensities ranged from darkness through scotopic to low photopic levels.

The detection threshold asymmetry found in earlier experiments was replicated with local stimuli. In contrast, however, the asymmetry between increment and decrement detection thresholds disappeared with fullfield stimuli. An ideal observer model was constructed to evaluate the role of two factors, Poisson variations and dark noise, in determining detection thresholds. Based on the model, these factors are insufficient to account for the increment-decrement asymmetry.

HELSINGIN YLIOPISTO
HELSINGFORS UNIVERSITET
UNIVERSITY OF HELSINKI

Tiivistelmä

Tiedekunta: Bio- ja ympäristötieteellinen tiedekunta

Koulutusohjelma: Neurotieteen maisteriohjelma

Opintosuunta: Neurotiede

Tekijä: Samu Tienhaara

Työn nimi: Valoinkrementtien ja -dekrementtien detektiokynnykset

Työn laji: Maisterintutkielma

Kuukausi ja vuosi: 05 / 2021

Sivumäärä: 53

Avainsanat: *Ihmisen näkö, Näköaisti, Psykofysiikka, Verkkokalvo, Detektiokynnys, Havaintokynnys, Inkrementti, Dekrementti*

Ohjaaja tai ohjaajat: Markku Kilpeläinen & Petri Ala-Laurila

Säilytyspaikka: HELDA – Helsingin Yliopiston digitaalinen arkisto

Muita tietoja:

Tiivistelmä:

Valonvälähdysten eli inkrementtien detektiokynnykset ovat korkeampia kuin valon vähenemien eli dekrementtien detektiokynnykset. Tätä asymmetriaa on usein selitetty sillä, että informaatio inkrementeistä ja informaatio dekrementeistä kulkeutuvat aivoihin eri neuraalisia reittejä, ns. ON- ja OFF-kanavia pitkin. Näillä kanavilla on tärkeitä rakenteellisia ja toiminnallisia eroavaisuuksia.

Tässä tutkielmassa toteutettiin koe, jossa koehenkilöiden inkrementtien ja dekrementtien detektiokynnykset mitattiin käyttäen sekä tilallisesti rajattuja ärsykkeitä (halkaisija 1,17 näköastetta), että rajaamattomia, koko näkökentän kattavia ärsykkeitä. Detektiokynnykset mitattiin psykofysikaalisella kahden intervallin pakkovalinta-menetelmällä. Taustavalona käytetyt intensiteetit vaihtelivat pimeydestä mataliin fotooppisiin valotehoihin.

Psykofysiikan kirjallisuudessa useasti löydetty asymmetria inkrementtien ja dekrementtien detektiokynnysten välillä replikoitiin lokaaleilla ärsykkeillä. Asymmetria kuitenkin hävisi täysin koko näkökentän kattavilla ärsykkeillä. Poisson-vaihtelun ja sauvasolujen spontaanin aktivaation roolia detektiokynnyksiin vaikuttavina tekijöinä tutkittiin ideaalihavainnoitsijamallin avulla. Nämä tekijät osoittautuivat mallin perusteella riittämättömiksi selittämään inkrementtien ja dekrementtien välisen asymmetrian.

Table of Contents

Symbols and Abbreviations

$[Ca^{2+}]_I$	intracellular calcium ion concentration
2IFC	two-interval forced choice task
cGMP	cyclic guanosine monophosphate
FWHM	full width at half maximum
LED	light-emitting diode
MLE	maximum likelihood estimation
ND	neutral density
PDE	phosphodiesterase
PW	peak wavelength
R*	photoisomerization
RGC	retinal ganglion cell
TLR	transformed likelihood ratio

Introduction

Our environment is a stormy sea of electromagnetic radiation. The nature of the waves in this sea, and their interactions with other properties of the physical world, has enabled animals across nearly all phyla to evolve a system that can extract information from a segment of the electromagnetic spectrum, known as the visible light spectrum. This extractable information is converted into neural signals by a largely conserved system, for which retina, a sensory organ in the eye, is acknowledged to be the starting point in mammals.

Visual sensitivity in low light levels

According to the nocturnal bottleneck hypothesis, early evolution of mammalian vision during the Mesozoic era selected for traits fit for an extended period of nocturnality (Hall, Kamilar, & Kirk, 2012). One such trait is high visual sensitivity in low light levels. There are nevertheless large differences among mammals in the emphasis placed on absolute sensitivity. The visual system of diurnal primates has evolved to prioritize other features over absolute sensitivity. Emphasis has been placed on visual acuity, but contrast sensitivity remains relatively high, even exceptionally so in daytime light levels (Harmening, 2017; Veilleux & Kirk, 2014).

The limits of human absolute visual sensitivity are well quantified. In a classic psychophysics experiment, Hecht, Shlaer and Pirenne (1942) set out to determine how many photons were required to reliably detect a light stimulus. After 40 minutes of adaptation to darkness, participants were exposed to flashes from a light that was positioned 20° temporally on the horizontal axis. Participants responded *yes* or *no* to indicate whether they saw the stimulus, and the intensity required for 60% detection rate was determined. Almost a complete absence of false positives was required from the participants. Only 54 to 148 photons were required to produce this level of detection (Hecht, Shlaer, & Pirenne, 1942). Not all photons reaching the cornea actually pass through the vitreous body and reach the retinal pigment epithelium, let alone produce excitations in photoreceptors. According to estimations calculated by Barlow (1977) and

updated by Donner (1992), a loss of photons occurs in the transmission of ocular media (25-50%), entering the photoreceptors (20-30%), absorption by rhodopsin (7-18%) and exciting the receptors (30-40%). It was originally estimated that 5 to 14 of the 54 to 148 corneal photons in Hecht et al. (1942) generated molecular changes that can activate a photoreceptor, i.e. photoisomerizations (R*). Subsequent independent analysis of the results has suggested an upper limit of only seven R* (Wald, 1991).

False positive rate is intimately linked to performance in a frequency-of-seeing experiment. With a more liberal requirement on the false positive rate, an observer can report seeing the stimulus without complete certainty. In another paramount experiment, at least one participant was able to perform above chance level at light intensities that were believed to produce only one R*, with a false positive rate of 29% (Sakitt, 1972). Additionally, the participant was able to rate light intensities on a scale of 1 to 7 on a linear scale, so that the ratings were believed to correspond to an equal actual amounts of R* plus noise events. Two other participants also performed at almost the same level. However, Sakitt (1972) appears to have vastly underestimated the fraction of photons at the cornea that end up generating an R*, by at least a factor of four (Donner, 1992). Thus, the lower limit estimate of circa five R* required for absolute detection threshold remains generally acknowledged.

The stimulus size used in Hecht, Schlaer and Pirenne (1942) was 10 angular minutes in diameter. The photons spread across a retinal area that contains less than 500 rods (Østerberg, 1935). If seven photons are absorbed randomly by these 500 rods, the probability that a single rod takes up more than one photon is only 4% (Hecht et al., 1942). After multiple trials, it can be statistically deduced that perception does not require two photons to be absorbed by the same rod. However, evidently some neural filter mechanisms at later stages of the visual system prevent a single photon alone from being consciously registered. Rather than a weakness, this can be considered an adaptive feature of the system. A system that registered every single photon would likely experience much more noise in very low light conditions. Spontaneous isomerization of rhodopsin molecules in rods is a very rare event, but the multitude of these molecules in a single rod give an isomerization rate of 0.2 per rod per minute (Baylor, Matthews, &

Yau, 1980). Each spontaneous isomerization produces a false positive, as these events are indistinguishable from light-activated events.

Early psychophysics experiments show that the variability of human responses to near-threshold visual stimuli is largely accounted for by the quantum nature of electromagnetic fields (Van Der Velden, 1946). Light is a Poisson process, where the amount of photons being emitted from a light source within unit time fluctuates around its mean λ, with variance $\sigma^2 = \lambda$. With increasing light levels, fluctuations increase sub-proportionally. At some point, the Poisson fluctuations can be considered negligible, yet they never cease to exist. Thus, any system that is intended to detect a stimulus is limited fundamentally by extrinsic noise.

Visual sensitivity as a function of three stimulus parameters

Background intensity. Weber's law states that the detection threshold is directly proportional to baseline intensity. Under the right conditions, detection thresholds of transient light increments are considered to follow Weber's law in the photopic range (Aguilar & Stiles, 1971; Blackwell, 1946). This is considered to reflect gain control mechanisms that enable constancy across a wide range of background light by avoiding saturation (Shapley & Enroth-Cugell, 1984).

With low background intensities, sensitivity is more crucial than saturation avoidance. In the scotopic range, detection thresholds follow the de Vries-Rose law. This law states that thresholds increase as a function of the square root of the background intensity, i.e. at a much lower rate than under Weber's law. Two alternative hypotheses explain this relationship. The law was independently discovered by de Vries and Rose, both of whom proposed that the inevitable variation in the amount of photons absorbed from a light sets a fundamental limit on observation, and that at the lowest light levels thresholds are limited by this factor (de Vries, 1943; Rose, 1948). This statistical model predicts the square root law. The fact that data fits this model suggests that detection thresholds are determined by these statistics (Barlow, 1957). An alternative hypothesis was posited by Donner et al. (1990), based on recordings from *Bufo Marinus* rod cells, bipolar cells and ganglion cells. The authors propose a model where thresholds are determined by two gain control mechanisms, a Weber gain mechanism in the rods and a

noise gain mechanism in the retinal ganglion cells (Donner, Copenhagen, & Reuter, 1990). In the low scotopic range, the Weber gain mechanism is inactive, but the noise gain mechanism sets a gain factor that is inversely proportional to the root-mean-square of the noise in the rod signals, resulting approximately in the de Vries-Rose law.

Stimulus area. Two other empirical laws, Riccò's and Piper's laws define the relationship between the spatial size and the perception of visual contrasts. According to Riccò's law, the difference in luminance, i.e. contrast, required for detection by human observers is inversely proportional to the angular area covered by the stimulus. This law applies only for uniform objects that are smaller than 0.4 degrees in visual angle (Barlow, 1958). For larger objects, the integrative mechanisms of retinal networks begin to play a role, and Riccò's law breaks down. For stimulus diameters between 0.4 and 20°, the detection threshold is governed by Piper's law, which states that the required luminance contrast is inversely proportion to the square root of the angular area (Piper, 1903). Both Riccò's and Piper's law apply for both absolute and relative thresholds.

Stimulus duration. Also noteworthy is that Hecht, Schlaer and Pirenne (1942) used short flashes of only one millisecond. It had been established at the time, that the duration of the stimulus and its luminous intensity at the absolute threshold are directly proportional, and that roughly the same amount of photons is required for detection regardless of the duration. This law of temporal summation is known as Bloch's law, or Bunsen-Roscoe law, and it broadly holds for stimuli shorter than 100 ms (Barlow, 1958). As the stimulus duration is stretched to one second, almost twice as many photons are required at the absolute threshold, as with <100 ms stimuli. Background intensity and stimulus area influence the boundary conditions for temporal summation. Bloch's law extends to slightly longer stimulus durations with the lowest background intensities. For large stimuli (27.6 square degrees), complete summation is followed by an abrupt transition to almost no summation at all. When the background intensity is high and the stimulus large, Bloch's range ends at 30 ms, after which hardly any temporal summation takes place (Barlow, 1958).

Retinal processing in visual detection

The phototransduction cascade is the process of conversion of light into neural signals. It starts by a photoreceptor, a rod or a cone, being activated by a photon-generated molecular change, a photoisomerization (R*). More precisely, a photon reaches and isomerizes the 11-cis retinal located in a g-protein coupled receptor known as opsin, which in turn is located on the cell membrane. The new structure of the retinal causes a conformational change in the protein, which activates a cascade of secondary reactions that results in activation of phosphodiesterase (PDE). This activated enzyme hydrolyzes cyclic guanosine monophosphate (cGMP) that closes the cell's sodium channels, effectively hyperpolarizing the cell. In short succession, voltage-gated calcium channels also close in response to the hyperpolarization. As a result of decreased $[Ca^{2+}]_I$, the release rate of glutamate-containing vesicles, that are calcium-dependent, also decreases. Ultimately, bipolar cells, that are downstream in the bipolar pathway (*Figure 1*), are depolarized because of the lower glutamate binding.

The visual system makes use of two types of classic photoreceptors – rod cells and cone cells. The phototransduction cascade of rod cells was already discussed above. Rod cells are scattered across the non-foveal areas of the retina, increasing in density from the fovea until the eccentricity of 18 degrees, and then gradually decreasing almost log-linearly (Østerberg, 1935). The size of rod photoreceptors, and the amount of convergence to downstream neurons also increase as a function of eccentricity (Goodchild, Ghosh, & Martin, 1996). Cone cells are located very densely in the fovea and are pooled minimally, thus enabling higher visual acuity. They come in three forms, giving the basis for color vision. The two types of photoreceptors distinguish the two visual subsystems, scotopic and photopic vision, that are generally found in humans and many other species. In dim light conditions, scotopic vision is mediated by the scarce photons activating rods, while cones remain silent. In brighter, photopic conditions, vision is mediated by cone cells. There is no exact illumination level, where the transition from photopic to scotopic vision happens, but rather an extensive zone called mesopic range characterizes the transition. For instance, most outdoor scenarios at night fall in the range of mesopic vision, where both rods and cones mediate vision (Puolakka et al., 2012).

The rod bipolar pathway (*Figure 1*) plays a key role in light detection under dark-adapted conditions. As a result of photoactivation, the glutamate release of hyperpolarized rod cells is transiently decreased from the intrinsic baseline release rate. The decreased binding to the postsynaptic mGluR6-receptors causes a depolarization in rod bipolar cells, that in turn release glutamate to excite AII amacrine cells. Convergence is high from the first connections of the pathway: each rod bipolar cell forms synapses with 20–50 rods, and each AII amacrine cell forms synapses with 20–25 rod bipolar cells (Taylor & Smith, 2004). The signal transmission can be modulated by horizontal cells (not depicted in *Figure 1*) providing negative feedback to cones and, less prominently, to rods (Thoreson, Babai, & Bartoletti, 2008).

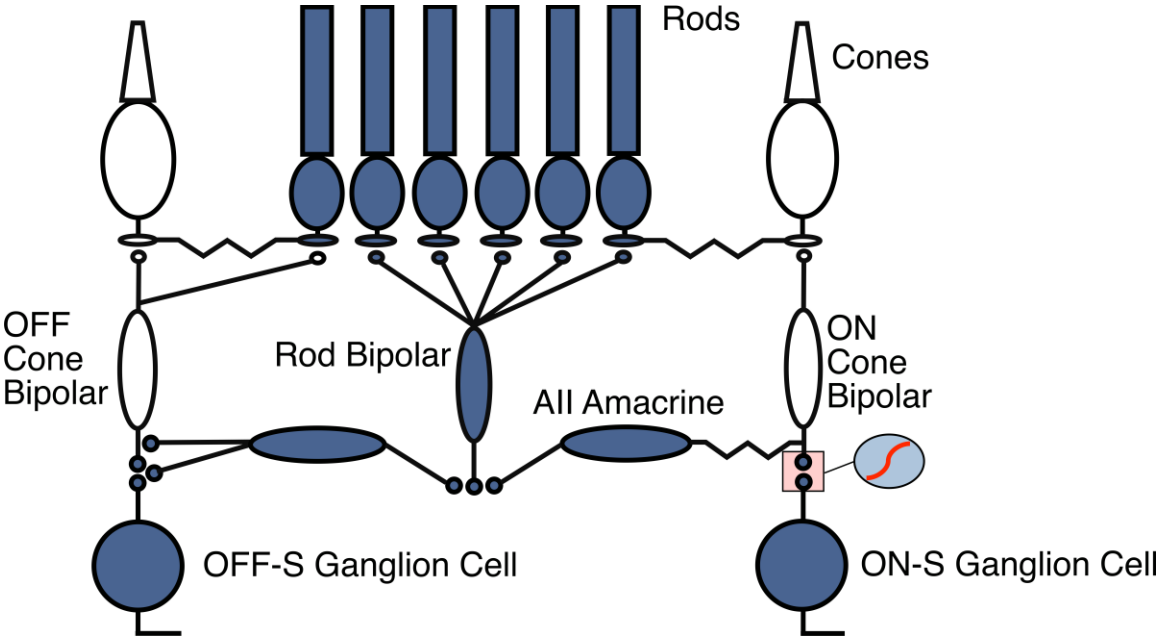

Figure 1. The rod bipolar pathway. This pathway conveys light signals in scotopic light levels. The pathway divides into two parallel streams. The ON pathway features a thresholding nonlinearity at the synapse between ON cone bipolar cells and ON ganglion cells.

From AII amacrine cells, the rod bipolar pathway diverges to two distinct pathways – an ON and an OFF pathway. AII amacrine cells transmit OFF signals via glycinergic inhibitory synapses to OFF retinal ganglion cells (RGC) directly, or indirectly by inhibiting OFF cone bipolar cells. ON signals are transmitted by exciting ON cone bipolar cells via dendro-axonal gap junctions (Volgyi, Deans, Paul, & Bloomfield, 2004).

The rod bipolar pathway is thus able to take over a part of the evolutionarily older cone pathway. Both types of cone bipolar cells subsequently transmit signals to RGCs. The ON pathway thresholds signals nonlinearly at the synapse between ON cone bipolar cell and ON RGC. Multi-photon signals lead to a depolarization of the ON RGC, generating an action potential, but single-photon events, as well neural noise are eliminated (Ala-Laurila & Rieke, 2014). In the OFF pathway, a signal from the OFF cone bipolar cell, or directly from the AII amacrine cell, causes a hyperpolarization in the OFF RGC, and a decrease in its baseline spiking rate. RGCs rely on action potentials to transmit signals through the optic nerve, but all the cells upstream to RGCs can use graded potentials to influence synaptic vesicle release rates. AII amacrine cells also utilize action potentials to at least some extent (Wu, Ivanova, Cui, Lu, & Pan, 2011).

In addition to the rod bipolar pathway, secondary pathways that bypass rod bipolar cells and AII amacrine cells have been identified. Rods also transmit signals via gap junctions to cone axons (Kolb, 1970; Raviola & Gilula, 1973), and directly to OFF cone bipolar cell dendrites (Soucy, Wang, Nirenberg, Nathans, & Meister, 1998). Nonetheless, for primates the primary rod bipolar pathway has been recognized as the dominant pathway, through which rod signals transverse up to background intensities where rods saturate and sensitivity sharply declines, around 300 R*/rod/s (Grimes, Baudin, Azevedo, & Rieke, 2018).

Besides extrinsic noise, reliability of single-photon responses is also limited by noise intrinsic to the rod phototransduction cascade (Baylor et al., 1980). The major types of signal-independent intrinsic noise are continuous noise and discrete noise (Field & Sampath, 2017). Both types stem from distinct components of the cascade. Continuous noise is the uninterrupted low-amplitude noise present in rod output. It is produced by at least two factors: PDE spontaneously activating and hydrolyzing cGMP, and spontaneous synthesis of cGMP by guanylyl cyclase. Discrete noise on the other hand stems from heat-activated isomerizations of rhodopsin molecules. It is relatively rare, large in amplitude, and indistinguishable from photo-activated rhodopsin isomerizations. While dim-light detection is primarily challenged by the nature of light, intrinsic noise is also a significant factor for absolute sensitivity, and is reflected as a phenomenological experience. Eigengrau, also known as dark light, is the uniform grey color that most

people report seeing in complete darkness (Wallach, 1948). Discrete retinal noise is believed to at least in part underlie this phenomenon (Baylor et al., 1980).

The asymmetry between increment and decrement detection sensitivity

Classic psychophysics experiments discovered an asymmetry between the detection thresholds for transient light increments, and for transient light decrements, at various background light levels (Blackwell, 1946; Short, 1966). The asymmetry consistently persists with stimulus durations up to 1 second (Patel & Jones, 1968). The asymmetry has been found across a wide range of background intensities and stimulus conditions. Lu and Sperling (2012) conducted 11 experiments on increment and decrement detection, using a wide variety of stimulus types, to evaluate the ubiquity of the asymmetry. Low photopic background luminances were used, ranging from 27 to 81 cd/m^2. An asymmetry was found in every experiment, with an average magnitude of 28% (ranging from 8% to 67%).

Not only are decrements detected at a lower threshold, but they are also processed with faster reaction time (Komban, Alonso, & Zaidi, 2011), higher visual acuity (Kremkow et al., 2014), and detected more readily on noisy backgrounds (Komban et al., 2014), although some of these effects are strongly modulated by the background luminance (Pons et al., 2017) and stimulus duration (Mazade, Jin, Pons, & Alonso, 2019). Rapid-off sawtooth stimuli are detected at a lower threshold than rapid-on sawtooth stimuli (Bowen, Pokorny, & Smith, 1989). One implication from this asymmetry is that humans read dark text on white background faster than they read light text on dark background (Buchner & Baumgartner, 2007).

The asymmetries between ON and OFF pathways have been proposed to give adaptive value to the statistics of natural scenes (Ravi, Ahn, Greschner, Chichilnisky, & Field, 2018). Dark and bright areas are non-uniformly distributed in natural scenes, and the asymmetries of the visual pathways are probably reflections of this (Cooper & Norcia, 2015). Compared to other encoding strategies, the fact that processing is divided into ON and OFF pathways enables more efficient information encoding (Gjorgjieva, Sompolinsky, & Meister, 2014). Furthermore, based on analysis of natural scenes, the optimal mosaic also entails an asymmetry between ON and OFF RGC receptive field

sizes, with smaller and more numerous OFF units (Ratliff, Borghuis, Kao, Sterling, & Balasubramanian, 2010). When building a mosaic of noisy linear-nonlinear neurons optimized for natural image information transmission, while minimizing metabolic costs, efficient coding principles predict multiple asymmetries in the organization of ON and OFF cells, and their filters (Karklin & Simoncelli, 2011).

Differences in the retinal processing of increments and decrements

The most studied retinal cells in the context of asymmetric processing of increments and decrements are mouse α RGCs, and their primate homologs, parasol RGCs. ON and OFF RGCs share overlapping receptive fields in a primate retina. When ON RGCs were pharmacologically silenced in a behaving primate, its ability to detect increments was heavily compromised. However, the animal's ability to detect decrements remained unimpaired (Schiller, 1992). The implication of this finding is that changes in luminance are processed separately by these two types of retinal ganglion cells, one increasing its activity as a response to increments, and the other increasing its activity as a response to decrements. Physiological evidence supports this idea (Pons et al., 2017; Zaghloul, Boahen, & Demb, 2003).

As distinct parallel pathways process increments and decrements, it is interesting to consider the differences in the anatomical and functional organization of these pathways. A body of evidence supports the assertion that these may drive the psychophysical asymmetry of detection thresholds. In macaque retina, OFF cone bipolar cells have been found to outnumber ON cone bipolar cells almost two-fold (Ahmad, Klug, Herr, Sterling, & Schein, 2003). As both RGC mosaics cover nearly the entirety of the retina, OFF RGCs must be distributed more densely than ON RGCs. ON RGCs thus also need wider dendritic fields. Indeed, the diameters of human ON RGC dendritic fields are 30-50% larger than their OFF counterparts (Dacey & Petersen, 1992).

Psychophysical asymmetries have been argued to be primarily a reflection of this asymmetry in RGC densities. This argument has its basis in individual ON and OFF RGCs in primates having similar sensitivity to increments and decrements (Benardete & Kaplan, 1999; Kremers, Lee, Pokorny, & Smith, 1993, as cited in Ahmad et al., 2003). It is also supported by light decrements being detected by humans with higher spatial

resolution, than light increments (Zemon, Gordon, & Welch, 1988). This interpretation remains to be confirmed, however. Other studies have found that when stimulated by light, individual ON and OFF RGCs show crucial differences in response dynamics and nonlinearity (Chichilnisky & Kalmar, 2002). These asymmetries may in turn be a consequence of the asymmetries in baseline transmitter release rates from presynaptic bipolar cells (Zaghloul et al., 2003). This difference in presynaptic input, as well as the difference in intrinsic conductances, might underlie other asymmetries between ON and OFF RGCs, such as that in spatial integration and spontaneous firing (Margolis & Detwiler, 2007; Turner & Rieke, 2016).

ON RGCs have been reported to process their scotopic input nonlinearly, relaying a thresholded code (Ala-Laurila & Rieke, 2014). In *Figure 1*, this is denoted by the red symbol at the synapse between ON cone bipolar cells and ganglion cells. On the other hand, OFF cells code information linearly at the lowest stimulus intensities in isolated mice and primate retinas (Takeshita, Smeds, & Ala-Laurila, 2017). In low photopic conditions, several additional functional asymmetries between macaque ON and OFF parasol RGCs have been found (Chichilnisky & Kalmar, 2002). In addition to nonlinear properties, ON cells were found to have 20% larger receptive field diameters and faster response kinetics. ON cells exhibited a graded response to decrements, but no similar response is seen by OFF cells to increments (Chichilnisky & Kalmar, 2002; Zaghloul et al., 2003).

In addition to asymmetries found at the level of RCGs, differences have also been found in the functional organization of the ON and OFF pathways. Cases of GABAergic crossover inhibition have been discovered between the two pathways for most cell types (Werblin, 2010). Crossover inhibition refers to the inhibitory signal being carried from one pathway to another via the AII amacrine cells. This crosstalk happens unidirectionally from ON to OFF cells, and not the other way around (Zaghloul et al., 2003).

At the lowest light intensities, ON pathway appears to shift its temporal tuning to lower frequencies (Pandarinath, Victor, & Nirenberg, 2010). When drifting grating stimuli were used to study temporal adaptation to photopic and scotopic light conditions, the optimal frequency for detection was lower with scotopic than photopic background

intensities. The tuning for decrements by the OFF RGCs remained the same across light range. An interpretation for these results is that with decreasing light intensities, the processing of increments in the ON pathway becomes slower.

It is unclear to which extent any of these differences influence downstream processing and become relevant for perception. Evidently, asymmetries between ON and OFF RGC readouts play a role in shaping readouts from the lateral geniculate nucleus, and ultimately the visual cortex (Jiang, Purushothaman, & Casagrande, 2015; Komban et al., 2014; Yeh, Xing, & Shapley, 2009). Presumably, these readouts shape the psychophysical asymmetry. Without manipulation of the observer's visual system, it is difficult to determine exactly which neural factors become relevant for the detection thresholds of increments and decrements.

Aim of the thesis

The aim of the current thesis is to investigate the nature of the increment-decrement asymmetry by testing whether it continues to exist when the stimulus size is not restricted to a small spot. To this end, a set of experiments was conducted, where increments and decrements were presented to a human participant both as fullfield flashes and as local spot flashes, across different baseline (background) light levels. The above-discussed literature leads us to wonder, whether the asymmetry persists when the stimulus area vastly exceeds the areas used in existing literature.

Another set of experiments carried out in the same lab (Koskela, Turunen, & Ala-Laurila, 2020) is particularly relevant to the current study. In these experiments, ON and OFF brisk-sustained alpha RGCs, that are the closest mouse equivalents to human parasol ganglion cells, were studied in dark-adapted, flat-mounted retinas. RGC detection thresholds were determined by patch clamp using 20 ms increments and decrements, similarly as intended in the present study, across dim background light levels. No asymmetry was found between increment and decrement detection thresholds, for either ON or OFF RGCs, with very low light levels.

The null hypothesis of the experiment is that increments and decrements are symmetrically detected at all light levels, with both fullfield and spatially restricted light stimuli. Light levels ranged from scotopic to low photopic. An ideal observer model was

constructed to compare the psychophysical findings to optimal performance, restricted by only Poisson distribution of light, and discrete retinal dark noise.

Methods

Participants

Five university students (three female; age 20-27, mean = 25.2) volunteered as participants in this study. The participants' level of sensitivity to dim lights was verified by a control session, during which detection thresholds for local stimuli in darkness were assessed, with a protocol essentially replicating the measurements of Hecht, Schlaer and Pirenne (1942). One out of six participants was deemed ineligible for the experiment due to insufficient sensitivity in this experiment. Participants 2, 4 and 5 were unaware of the hypotheses of the study. All participants had normal vision without correction. The study adhered to the principles of the Declaration of Helsinki and was deemed ethically acceptable by the Ethics Review Board in the Humanities and Social and Behavioural Sciences of the University of Helsinki. The participants signed written consent, prior to the experiment.

Apparatus

To enable presentation of both global and local stimuli, a ganzfeld globe was used. Three light-emitting diodes (LED) were set up around the globe: one for fixation (*AND180HRP*; interference filter by Melles Griot 03 FIV 125; peak wavelength (PW) = 680 nm; full width at half maximum (FWHM) = 10 nm), one for local stimuli (Spot LED; *AND520HB*; interference filter by Edmund Optics (#65-149); PW = 500 nm; FWHM = 10 nm) and one for global stimuli (same LED and filters as for the local stimuli). Mounted optical diffusers (global stimuli: Newport Corporation; 10DIFF-VIS; local stimuli: Thorlabs ED1-C20-MD) were used to scatter the incident light uniformly. A set of Thorlabs absorptive neutral density (ND) filters was used to achieve the desired intensity range. A crosshair shaped aperture was situated before the fixation stimulus. A PC running MATLAB (The MathWorks) was used to control all stimulus presentation and data acquisition. The LEDs were connected to the computer via a *National Instruments USB-6343 DAQ* system and an LED driver.

Stimuli were viewed monocularly. The participant had his/her left eye covered by a patch, and the viewing distance and angle were controlled with a chin rest, that was carefully situated prior to each session to ensure correct position of the eye with respect to the spot LED. The participant was seated on a swivel chair, with a keyboard on his/her lap. Essential parts of the setup are illustrated in *Figure 2*.

The inner surface of the ganzfeld globe was extremely diffuse and reflective, so that it was equiluminant across the visual field. Outside the duration of flashes, the spot and the background (the ganzfeld surface) were also equiluminant. This equiluminance was validated with the use of a high-performance camera (*Andor Zyla 4.2 sCMOS*).

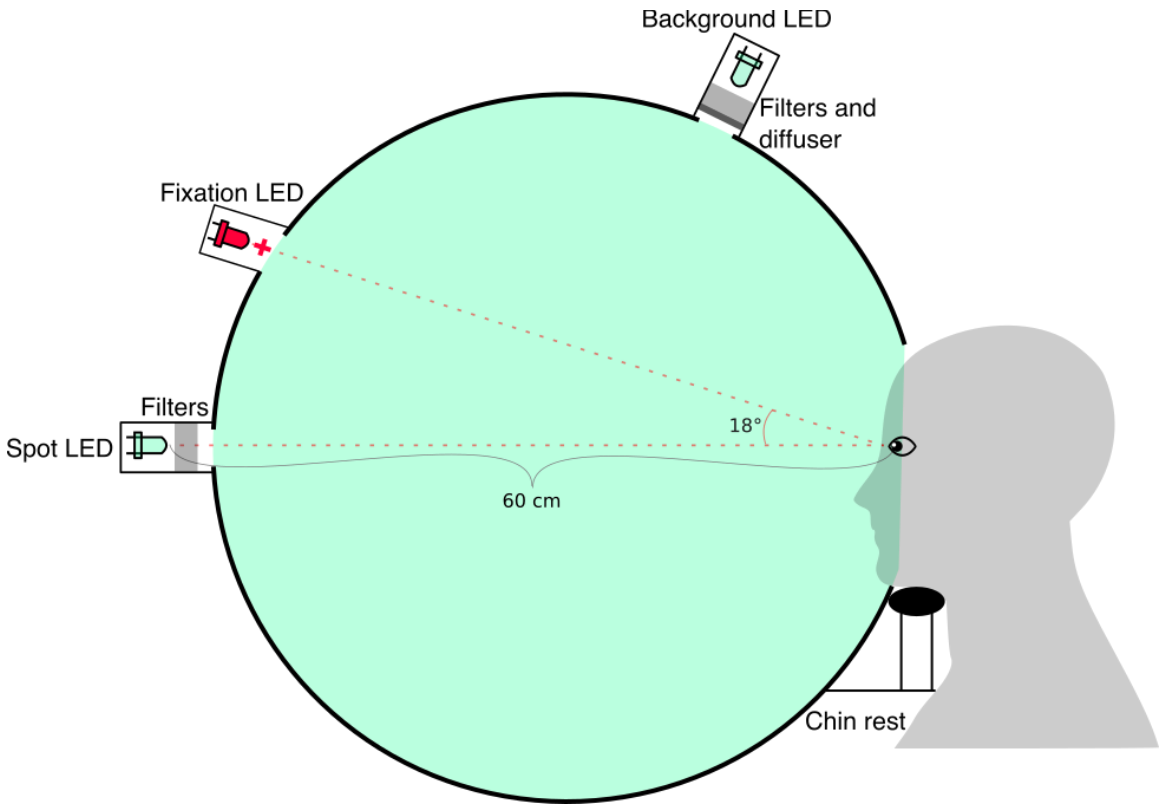

Figure 2. Ganzfeld setup. The participants fixated their gaze on the red Fixation cross. The Background LED was not in the participant's direct field of vision. The inner surface of the ganzfeld globe was highly reflective, so that the Background LED created an equiluminant fullfield stimulus.

Stimuli

The participants completed the global detection task in a total of 11 conditions; 2 classes of stimuli, increments and decrements, with 5 different baseline light intensities, and an increment detection task with no baseline light. The baseline light intensities were set apart by roughly one log unit. Individual variability to baseline light intensities was introduced by the decline in LED efficiency over time, and the switching of the LED. These factors were controlled for by regular calibration of the light sources.

The local detection task was completed only with the brightest baseline light condition, and in the darkness. An exception to this was participant 3, who also completed the local detection task in conditions that were 1 log unit lower, and 50% higher than the highest baseline condition. The participant fixated on the fixation LED, which placed the spot LED at 18-degree eccentricity. The size of the spot stimulus was restricted by an aperture, so that from a viewing distance of 60 cm, the diameter of the stimulus covered 1.17 degrees of visual angle.

Light conversions

The pupil is an adaptive aperture that controls the light intensities, i.e. the amount of photons that arrive at the retina. For participants 1, 2 and 3, pupil sizes in different baseline light conditions were measured with *Andor Zyla 4.2* camera to control for this effect on the actual light intensities. A dim infrared light was used to measure the pupil size in darkness. The measuring conditions were set up to mimic the conditions of the actual experiments. After obtaining three video clips of 20 seconds in each light level, the pupil size was analyzed by a circle detection algorithm, which was robust for confounders such as blinking and eyelids covering a part of the pupil at times. The size of each pixel was determined by taking pictures of the participant holding a ruler next to his/her head. Stages of the pupil size analysis are illustrated in *Figure 3*.

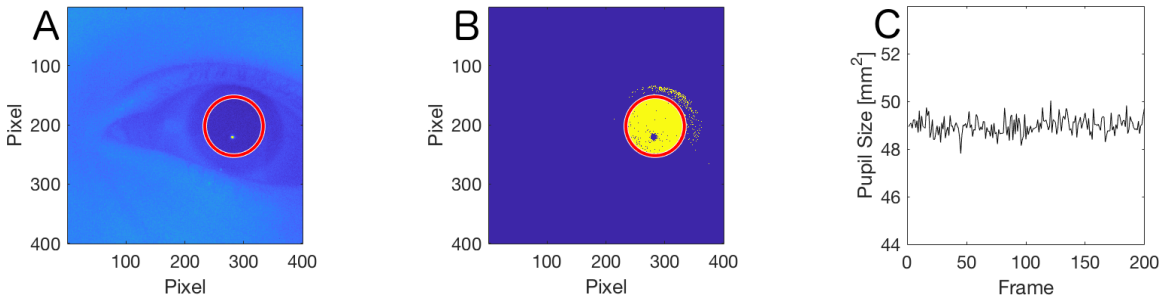

Figure 3. Method of determining pupil sizes. (A) Example of a raw frame. (B) The same frame with thresholding applied. The pupil is encircled using a circle detection algorithm. The same circle overlaid on (A). (C) Pupil sizes detected in each frame of a 20 second recording.

A regression analysis was performed on median pupil sizes derived from each separate video clip. Significant regression was found ($F(1, 13) = 21.6\text{-}76.5$, $p < 0.001$), with R^2 values between .625 and .855. For conditions with a non-zero baseline light, the fit line was used for pupil size adjustments in luminance calculations. Pupil sizes measured in darkness were not used for the fitting, but their average was used in calculations instead. An example of the fitting is presented in *Figure 4.* Pupil sizes for each participant are presented in *Table 1*.

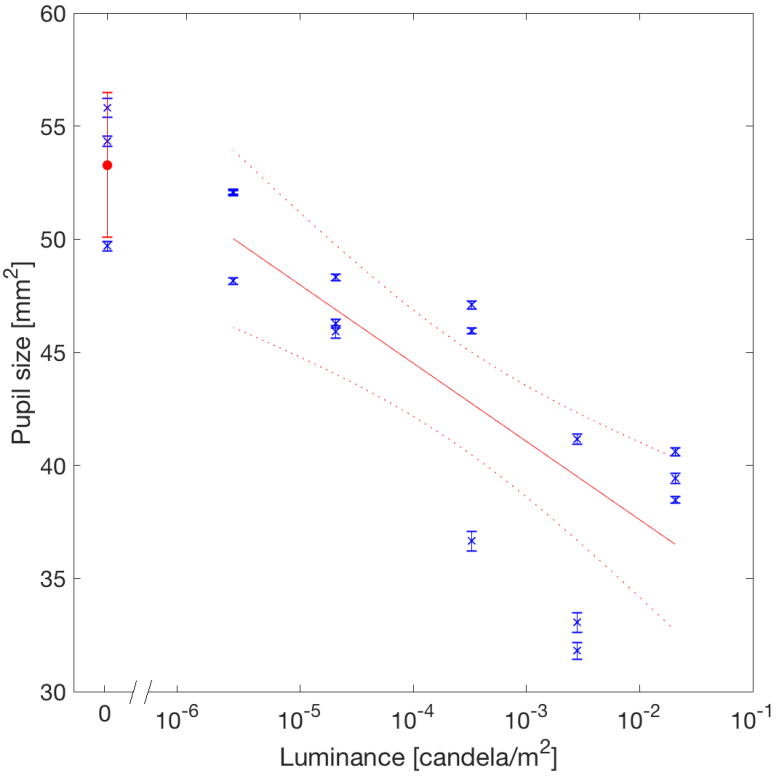

Figure 4. Logarithmic regression, predicting pupil size by background luminance. Three video clips were recorded in each condition, represented by the blue data points. The red circle denotes the mean pupil size in darkness. Participant 2.

Table 1

Participants' pupil sizes in different baseline light conditions. Values based on the regression analysis, except for the condition in darkness.

	Pupil size (mm^2)		
Luminance (*log. cd/m*^{2})	Participant 1	Participant 2	Participant 3
Darkness	42.6	53.3	43.4
-5.59	40.8	49.7	44.7
-4.69	39.2	46.7	43.2
-3.48	37.0	42.7	41.2
-2.55	35.3	39.6	39.7
-1.69	33.7	36.7	38.3

Stimulus intensities were regularly calibrated. Calibration was conducted by first measuring the luminance yielded by maximum voltage and with no filters mounted, using a photometer (*Minolta LS100*). Non-linearity of the LED was quantified by measuring the produced irradiance with a radiometer (*UDT Instruments S471*) across a wide range of voltages. These data were fit with a polynomial function, the inverse of which was used to linearize the stimulus setup.

Voltage input for the LED lights was converted to photoisomerizations in rod-cells with the following conversion steps and assumptions:

1. Measured amount of power in watts at the cornea based on radiometer and photometer measurements, without filters.
2. Multiplication of this power value by the duration of a stimulus, i.e. 0.02 seconds, to get energy in joules-per-stimulus.
3. As per the equation for photon energy, $E = hf$, where h is the Plack constant, and f is the frequency of the photon, a photon propagating with the wavelength of 500 nm has the energy of 3.97289e-19 joules. The above-mentioned joules-per-stimulus is then divided by this amount, to get photons-per-stimulus.
4. Multiplication by filter attenuation factor. Exact ND and interference filter attenuation factors were obtained by radiometer measurements.
5. Multiplication by the pupil diameter, and the quantum catch factor, calculated by Donner (1992). Quantum catch gives the fraction of the light quanta at the corneal surface that enter through the pupil and are absorbed by retinal, subsequently activating rod cells. This thesis uses the lower boundary value of Donner's estimations: 0.17. Eccentricity of the stimulus with respect to the eye was 18 degrees dorsally, in order to maximize the density of rods to be exposed to the light quanta (Østerberg, 1935). At this eccentricity, out of all the photons reaching the cornea, 17% are estimated to produce effective isomerizations in the retina.

As a result of calibration, switching of LEDs, and most importantly differences in pupil sizes, variance was introduced to the used background and stimulus intensities

between the participants. Mean background intensities in R*/rod/second are presented in Table 2, for every condition used in the global and local detection task.

Table 2

Mean background intensities (M) and ranges in R/rod/second used in all conditions of the 2IFC detection task.*

	Global						Local		
	Dark	1	2	3	4	5	Dark[a]	5[b]	5+[c]
M	0	.00518	.0393	.602	4.98	37.3	0	36.7	56.2
Range	0	.0043-.0067	.0319-.0500	.482-.728	3.94-5.79	30.5-40.7	0	30.5-40.7	56.2

[a] Data from only 4 participants
[b] Data from only 3 participants
[c] Data from only 1 participant

Procedure

Each session began with a 30-minute dark adaptation period. In experimental conditions where non-zero baseline lights were used, the dark adaptation period was followed by ten minutes of adaptation to that baseline light level. After that, the actual experimental session comprising a two-alternative forced choice task began. This method of psychophysics was developed to measure sensitivity to sensory input by making the observer choose between two versions of the stimulus. When the two versions are presented sequentially, the method is also known as two-interval forced choice task (2IFC). *Figure 5* presents a graphic illustration of the stimuli used in a single trial of the local decrement and global increment detection task. One trial proceeded as follows. The participant had his/her gaze directed at the fixation LED that blinked (turned completely off for 40 ms) four times, with 500 ms intervals (Column B in *Figure 5*). On either third or fourth of these flashes, either a light increment or a decrement occurred in either of the other two LEDs, depending on the experimental condition (global or local; Column C in *Figure 5*). In *Figure 6*, the light intensities of the three LEDs are plotted against time. The participant's task was to indicate by a key press, whether he/she saw the stimulus on

either the third or the fourth flash of the fixation point. After a response was given, the next trial was initiated.

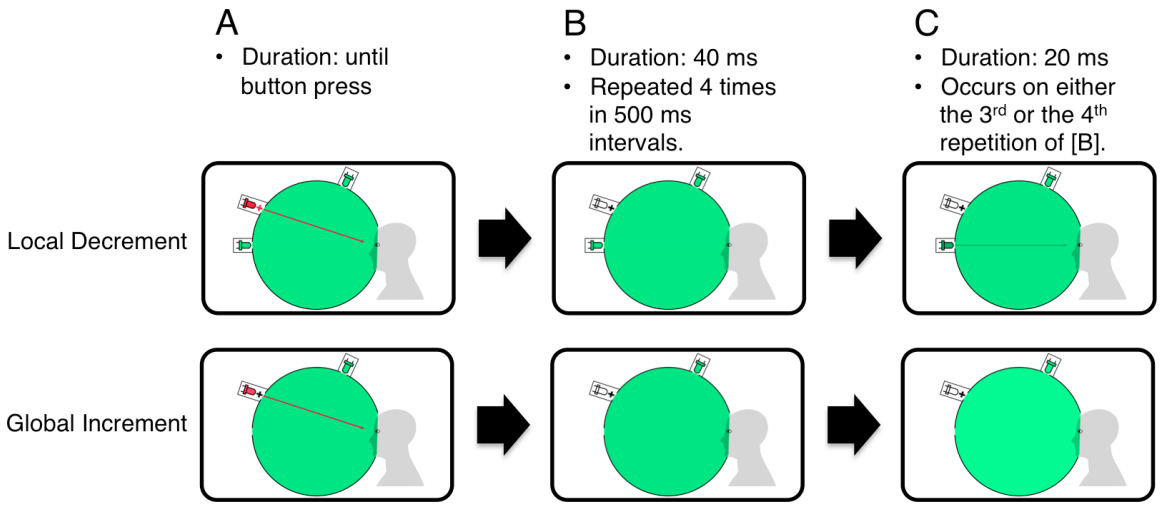

Figure 5. Schematic illustration of the experimental task. (A) The baseline condition of the task. When a button is pressed, a blink of the fixation cross (B) is presented for 40 ms for four times, with 500 ms intervals. On either 3rd or 4th repetition of the blink (B), the stimulus (C) is presented for 20 ms. The goal of the participant is to detect whether the (C) occurs on repeat 3 or 4.

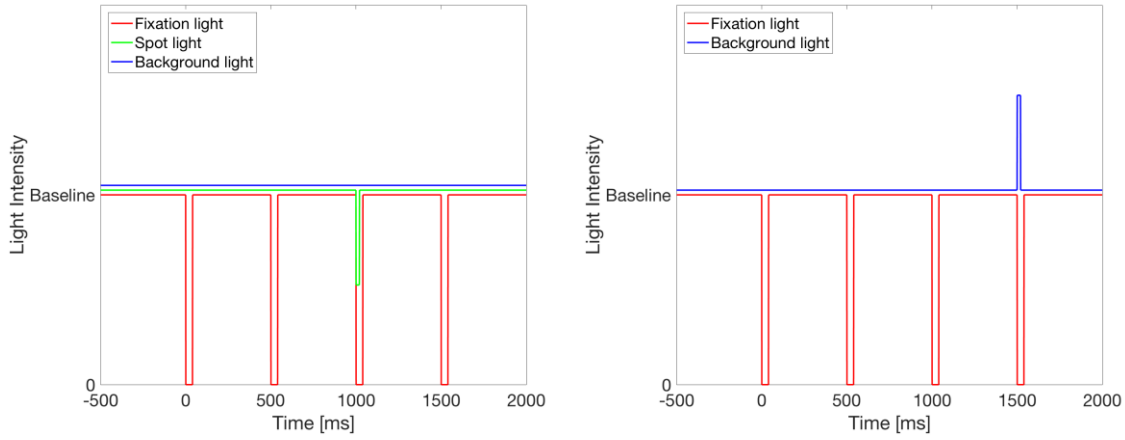

Figure 6. Intensity of used lights as a function of time. The left plot illustrates an example trial of the local decrement detection task, and the right plot illustrates an equivalent global increment detection task.

Six different stimulus intensity classes were used in every condition, in a randomized order. The seventh "intensity class" was a so-called sham stimulus, where no

increment/decrement was presented. If the lowest intensity class did not correspond to a ~50% correct response rate, or if the highest intensity class did not correspond to a 100% correct response rate, the intensity classes were readjusted. Typically one such adjustment was required at the beginning of every session. A session consisted of ~100 trials per intensity class, and was divided into 5 to 15 blocks. Correct response rates were monitored between every block.

Data analysis

For every experimental session, the rate of correct responses was determined for each intensity class. A psychometric function can be constructed by fitting a normal cumulative function to the data. Psychometric functions were fitted with the use of MATLAB software, and an analysis toolbox *Palamedes* (www.palamedestoolbox.org), by means of maximum likelihood estimation (MLE). Confidence intervals to the plots were estimated using bootstrapping. In this method, a large amount of samples is drawn randomly and with replacement from the original data. A psychometric function is fitted to each of these samples, giving a sampling distribution for each stimulus intensity value. The standard deviations of these sampling distributions give the confidence intervals for each condition. In the present analysis, each condition was simulated with 400 iterations. The psychometric functions in *Figure 7* were constructed by this method. One useful feature of such functions is that the 75% detection threshold can be directly observed, and is illustrated by the dashed line in *Figure 7.* In all subsequent figures relating to thresholds, the data points represent stimulus intensities required for this performance level. A characteristic analysis code transforming participant responses to psychometric functions can be found at https://github.com/Kapsalon/Ganzfeld (Example for analysis of global increment and decrement detection. Modified pipelines were applied for other experiments).

The participants who completed both local and global detection tasks were included in the statistical analysis. Transformed likelihood ratio (TLR) test was used in statistical analysis. TLR test is a model comparison test that evaluates whether differences between psychometric functions can be attributed to actual differences in the dependent variable, or are due to the sampling error alone. By applying a maximum

likelihood criterion that is based on the observations, we can estimate parameters for two nested models. Likelihood ratio tests compare these two models, the so-called fuller and a lesser model. The key parameter in this analysis is the 75% detection threshold, which under H_0 is the same for both increment and decrement stimuli. The lesser model is more restrictive, and in this case assumes a single threshold value based on all observations. The fuller model allows the thresholds to be different in each condition. In the test, each model is fitted to the data by means of MLE. The ratio between the likelihood under the lesser model and under the fuller model, determines the likelihood ratio (Kingdom & Prins, 2016).

For the purposes of model comparison tests in psychometrics, likelihood can be defined as the probability with which a hypothetical observer, operating under parameters set by the model, would perform exactly like a human observer. The likelihood is used for the procedure of maximum likelihood estimation, and serves as a metric that defines parameters for the "best-fitting" model. Likelihood ratio is a statistic that is calculated as follows:

$$LR = 2(logL|\widehat{\theta_{ML}}) - logL(\theta_{H_0}) \qquad (1),$$

where L is likelihood, $\widehat{\theta_{ML}}$ is the maximum likelihood estimates of the parameter, and $L(\theta_{H_0})$ is the likelihood if the null hypothesis is true. Likelihood ratio is often reported in a monotonically transformed form, referred to as transformed likelihood ratio:

$$TLR = -2 * log_e(LR) \qquad (2).$$

The results section concludes with an ideal observer analysis. The participants' task performance was compared to that of an ideal observer model. The model's performance was restricted by only the Poisson distribution of photons, and by the dark noise rate of human rods. The dark noise rate used here was 0.0038 events per second per rod, an average value from the range of estimations in literature (Field, Sampath, & Rieke, 2005).

Results

When the stimulus was a small spot (diameter 1.17 degrees of visual angle), the detection thresholds were consistently higher for increment than for decrement stimuli. This is in line with many earlier studies (Blackwell, 1946; Short, 1966). The average difference was 0.158 log units (*SD* = 0.018), or 44.0% (*SD* = 5.9). Proportion of correct responses are plotted against the stimulus intensities in *Figure 7.* In the figures, standard deviations of the parameter estimates resulting from the simulations are illustrated by the shades around the psychometric functions.

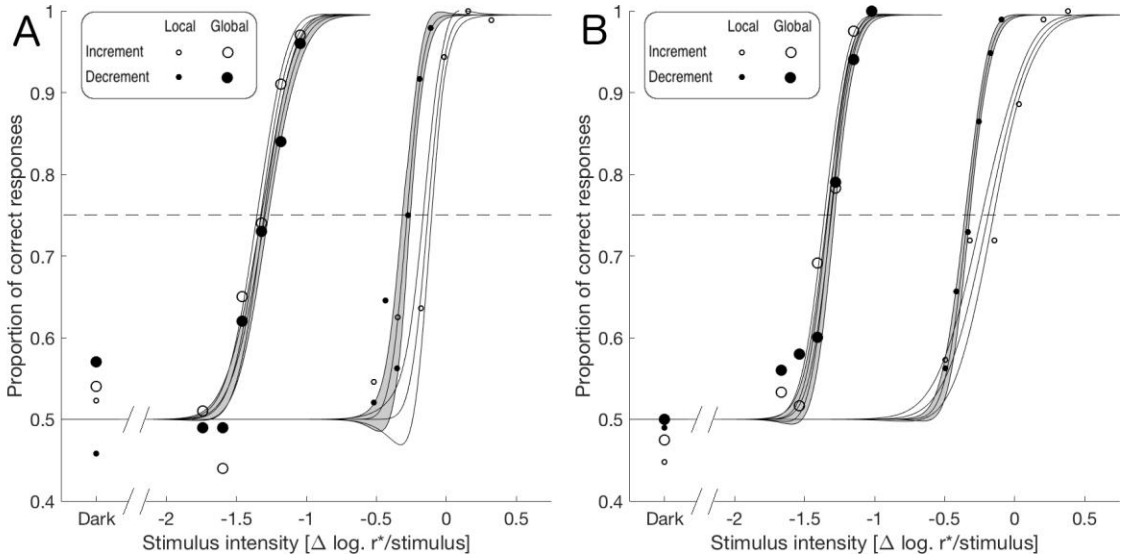

Figure 7. Correct response rates in a 2IFC task as a function of stimulus intensity for increments and decrements of two stimulus types, global and local. Data points furthest to the left, before the x-axis cutoff, represent sham stimuli. The sham stimulus data were not used for fitting. (A) Participant 2; Baseline ≈ 38.62 R*/rod/s for local stimuli, 38.84 R*/rod/s for global stimuli. (B) Participant 3; Baseline ≈ 40.42 R*/rod/s for local stimuli, 40.65 R*/rod/s for global stimuli.

Psychometric functions depicted in *Figure 7* provide a representative example of all data. A strong symmetry between increment and decrement thresholds was found for global stimuli (large symbols) across all baseline light levels. A robust asymmetry, in contrast, was found for local stimuli (small symbols). With low baseline light levels, the participants were not able to detect even total decrements, i.e. decrements to full

darkness. Participants were found to be too insensitive to reliably perform the local decrement detection task with baseline lights dimmer than 38 R*/rod/second, and for this reason, only one baseline light level was used for local detection tasks.

To test tentatively whether the asymmetry between local detection thresholds would persist with lower baseline lights, participant 3 completed a 2IFC task with a baseline light of 5.8 R*/rod/s, consisting of 336 trials of total decrements only, including 48 sham stimulus trials. A performance level of 75.7% correct was achieved. With incremental stimuli of equivalent intensity, the performance level remained at chance level (45.6%), consistent with the result with the higher baseline intensity. Participant 3 also completed the local detection task with a slightly higher baseline intensity of 56.23 R*/rod/s. The thresholds here were 0.811 R*/rod (*SD* = 0.070) for increments and 0.751 (*SD* = 0.033) R*/rod for decrements. These data points are shown in the upper right corner of the *P3* plot in *Figure 8.* Error bars presented in all plots represent a single standard deviation.

With local stimuli, increment thresholds were more than 40% higher for every participant than the decrement thresholds with the same baseline light. No such asymmetry was observed with global stimuli. For the comparison's sake, using the same background intensity with which the local detection thresholds were measured (*M* = 37.3, *SD* = 3.9 R*/s), the global increment thresholds were on average 3.3% (*SD* = 8.6) higher than the global decrement thresholds. Also, across all background intensities global thresholds were roughly the same – on average, decrement thresholds were higher by only 1.8% (*SD* = 11.1). The differences between the thresholds are presented more elaborately later, in *Figure 9*. Mean thresholds for every condition are presented in *Table 3*.

A comparison between local and global thresholds shows that more total R* are needed for global thresholds than for local thresholds. On average, global thresholds were higher than local thresholds by 2.89 (*SD* = 0.12) log units for increments and 3.06 (*SD* = 0.14) log units for decrements. In terms of R* per rod cell, global thresholds are lower. This difference was 1.13 (*SD* = 0.11) log units for increments, and 0.96 (*SD* = 0.14) log units for decrements. *Figure 8* shows these differences in R* per rod for participants 1, 2 and 3 separately.

Thresholds of each participant plotted against background intensities are somewhat sigmoidal (*Figure 8).* The slopes are at their steepest between the three middle background intensities. The average slope between the second and third brightest condition is 0.91 for increments (range: 0.77-1.08) and 0.96 for decrements (range: 0.84-1.11). The average slope between the conditions with the lowest and the second lowest background intensity is 0.57 for increments (range: 0.47-0.65) and 0.54 for decrements (range: 0.41-0.63).

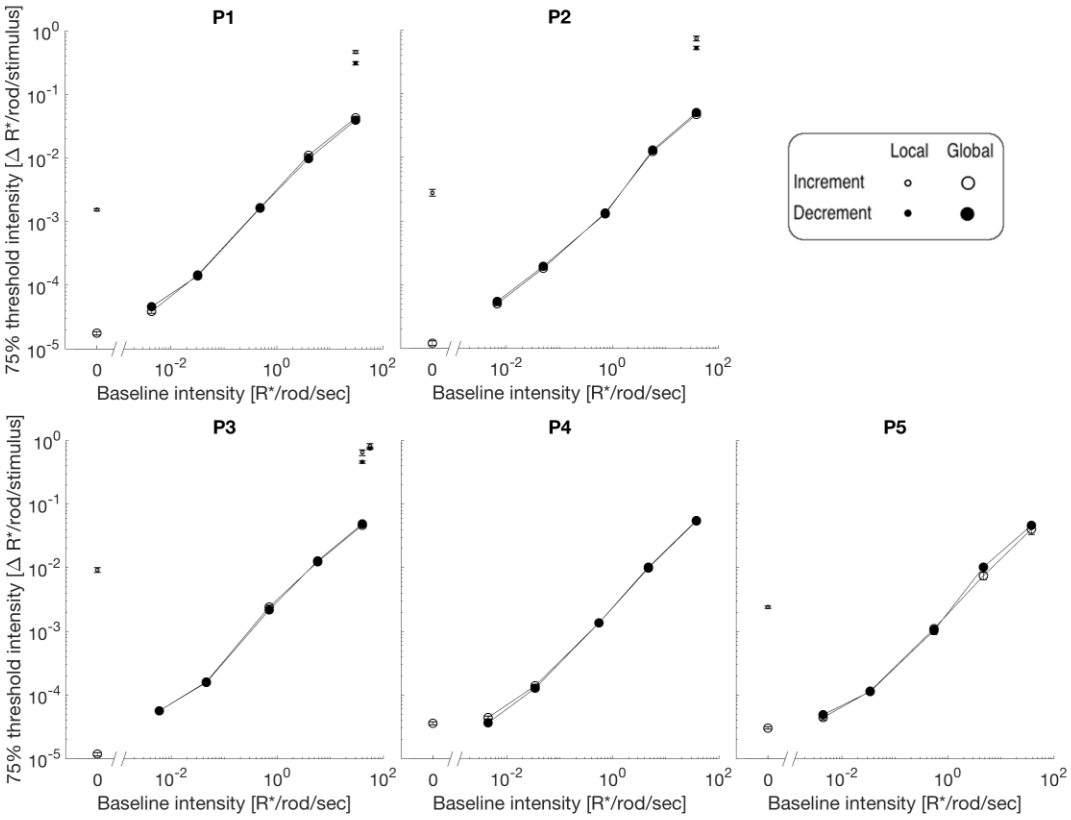

Figure 8. Detection thresholds as a function of background light level for all participants. Experiments with local stimuli were not conducted for participants 4 and 5, apart from the local detection task with no baseline light for participant 4. Additional data was measured for participant 3 with baseline intensities exceeding the otherwise brightest conditions by 40%. The error bars (1 SD) are too small to be seen in the figure as the markers occlude them.

Table 3

Mean (M) thresholds and standard deviations (SD) in R/rod for increment and decrement detection thresholds in global and local 2IFC tasks.*

Baseline intensity (*M*; R*/rod/s)	Increments		Decrements	
	M	*SD*	*M*	*SD*
		Global thresholds		
Dark	2.16×10^{-5}	1.11×10^{-5}		
0.00518	4.66×10^{-5}	6.76×10^{-6}	4.82×10^{-5}	7.86×10^{-6}
0.0393	4.18×10^{-4}	2.49×10^{-5}	1.46×10^{-4}	3.09×10^{-5}
0.602	.00158	.00051	.00150	.00044
4.98	.0106	.0011	.0112	.0015
37.3	.0463	.0054	.481	.0060
		Local thresholds		
Dark[b]	.00399[a]	.00354[a]		
36.7[c]	.617	.140	.431	.111
56.2[d]	.811	N/A	.751	N/A

[a] Data features an outlier. Excluding the outlier, $M = .00224$, $SD = .00065$.
[b] Data from only 4 participants.
[c] Data from only 3 participants.
[d] Data from only 1 participant.

With global stimuli, increment and decrement thresholds are essentially identical across all baseline light levels; deviances from symmetry are modest and go in both directions, and are thus more likely predominantly due to random error. With local stimuli, however, decrement thresholds are lower than increment thresholds. These data are depicted in *Figure 9*, where the relative differences between increment and decrement thresholds are plotted against the baseline light intensity for participants 1, 2 and 3. The values on the y-axis are derived by dividing the increment thresholds by the decrement thresholds. Error bars represent standard deviations of the ratios, and were calculated as advised by Elandt-Johnson & Johnson (1980) and Stuart & Ord (1998).

A statistical analysis was performed to evaluate the symmetries between increment and decrement thresholds, illustrated in *Figure 9*. The decrement thresholds were lower than increment thresholds for all participants that completed the local task,

with differences ranging between 40.4% and 50.9%. The difference is statistically significant for all observers (TLR test, $p < .001$). For participant 2, the p value is based on an incomplete set of simulations due to unsuccessful convergence. Nevertheless, even if all six failed fits yielded higher transformed likelihood ratios than the experimental data, $p = .003$ (lower than α) would still be obtained.

Conversely, no significant asymmetries were found between the detection thresholds in the global conditions for these same participants. As the global thresholds were compared in five conditions, a Bonferroni correction was applied and a significance threshold $\alpha = .01$ was used. The differences between these thresholds ranged between 1.2% ($p = .91$) and 15.2% ($p = .06$). Again, some of the sets of simulations were incomplete. Regardless, all of the differences were sufficiently small, and thus the small number of unconverged fits can be disregarded and the null hypothesis safely retained. Even under the most conservative assumption, that none of the six unconverged fits had a greater likelihood ratio than that obtained from the observations, the p value does not fall below .04.

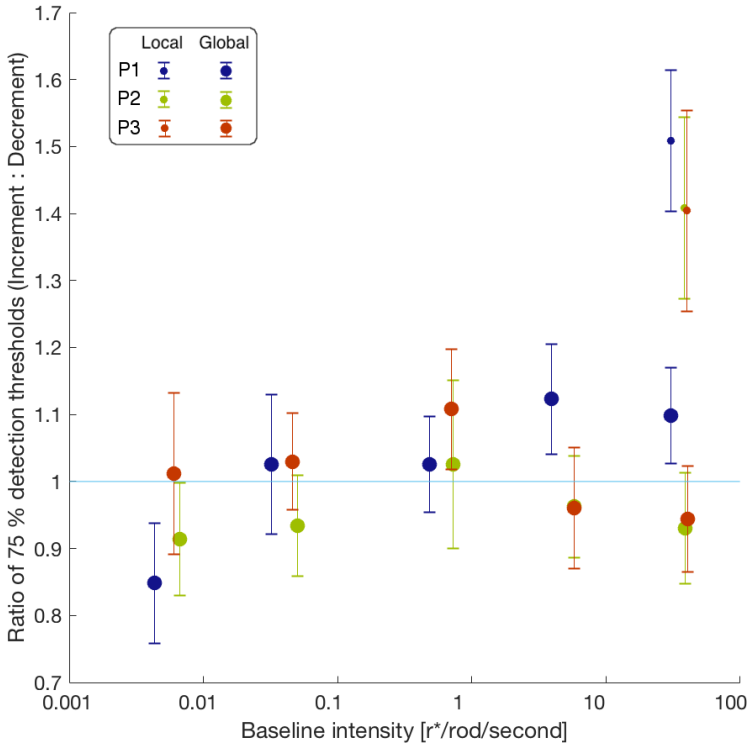

Figure 9. Detection threshold asymmetries. Increment thresholds relative to decrement thresholds as a function of baseline intensity.

Performance of participants 1, 2 and 3 was compared with the optimal performance of an ideal observer model. The model performs the theoretical 2IFC detection task. In this case, model performance was constrained only by two factors: the Poisson distribution of light, and the dark noise rate of the detectors.

The Poisson distribution of light sets the ultimate limit on visual sensitivity. Incident photons are independent events with a random temporal distribution. Hence every photon counter, real or theoretical, is constrained by the Poisson distribution of photon counts.

For a mean number *a* R* in a cell array, *P(r|a)* denotes the probability that the number of R* in a given light interval is exactly *r*:

$$P(r|a) = \frac{a^r}{r!} e^{-a} . \quad (3)$$

When time interval t over which the photons are measured is considered, the process is described by

$$P(r|A) = \frac{(At)^r}{r!} e^{-At} , \quad (4)$$

where *A* is the mean rate of R* per second. To understand the simulations presented here, consider *Equation 3, 4* and *5* to correspond to intervals in the 2IFC paradigm that contain the baseline intensity only, with no increment or decrement stimulus.

In any given trial, the mean number of photoisomerizations *a* can be considered to be governed by two factors: *n*, the mean quanta measured at the cornea, and *q*, the quantum catch, the probability of a corneal photon to produce an R* after attenuation due to the optical properties of the eye and the retina. Photons at the cornea follow a Poisson distribution with mean *n*. The probability for a corneal photon to produce an R* is *q*. In effect, each value of photon distribution is passed through a binomial filter, where the probability of each independent event passing is *q*. This results in a variable that is also Poisson-distributed, with mean *qn* (Teich & Saleh, 1982; Tiihonen, 2019).

Besides photon statistics, the performance of an ideal observer is unavoidably constrained by spontaneous, discrete activations of rhodopsin molecules. These events are indistinguishable from real photon absorptions, and therefore limit sensitivity. Like photon absorptions, these activations follow a Poisson distribution, and in complete darkness their mean is *x*. Due to this noise, an ideal observer is expected to mistake a "blank" interval for a light flash in some proportion of the trials. With a baseline intensity of *q* corneal photons, the mean number of R* is caused by light absorption, *qn*, and by the dark noise, *x*. The sum of these terms has a mean $a_0 = qn+x$ and also follows a Poisson distribution, as *n* and *x* are both independent Poisson-distributed random variables (Teich & Saleh, 1982). In the current model, a dark noise rate of $x = 0.0038$ was used. Thus,

$$P(r|a_0) = \frac{(qn+x)^r}{r!} e^{-(qn+x)} . \quad (5)$$

When a trial contains a stimulus, its intensity in corneal photons, *s*, can be added to *n*. The sum of these variables is referred to as a_1. The variable *s* has a positive or a negative value, depending on whether the stimulus is an increment or a decrement. The probability that the response to a trial with stimulus a_1 is exactly *r* isomerizations is

$$P(r|a_1) = \frac{(q(n+s)+x)^r}{r!} e^{-(q(n+s)+x)} . \quad (6)$$

In a 2IFC paradigm, the objective of the observer is to indicate which of the two intervals contains the stimulus. The intervals with stimuli, and the intervals with no stimuli can both be considered to be samples from two distributions of neural responses. An ideal observer can systematically choose the larger of the two responses, or smaller in the case of decrements. The proportion of correct responses is the probability that the sample drawn from the signal + baseline + noise distribution is larger than the sample drawn from the baseline + noise distribution, plus half of the probability of two samples being equal. Using *Equations 5* and *6* described above, the proportion of correct responses is given by

$$P_c = \sum_{r=0}^{\infty} P(r|a_0) \sum_{u=r+1}^{\infty} P(u|a_1) + 0.5 \sum_{r=0}^{\infty} P(r|a_0)P(r|a_1)\,. \qquad (7)$$

In the case of decrements, P_c is the probability that the sample drawn from the signal + baseline + noise distribution is smaller than the sample drawn from the baseline + noise distribution. Effectively, in *Equation 7*, the positions of a_0 and a_1 become reversed in the first term.

Equation 7 gives P_c for one stimulus intensity (a). The 75% detection threshold can be obtained by finding the intensity that yields a P_c of 0.75. To compare human observers with ideal observers, these 75% detection thresholds were plotted as a function of background intensity in *Figure 10*.

The thresholds of human observers exceed those of ideal observers more than an order of magnitude in every condition. In darkness, the threshold values of the ideal observer were 1.04×10^{-4} R* for local stimuli and 7.61×10^{-7} R*/rod for global stimuli, falling below human observer thresholds by 1.49 and 1.41 log units, respectively. At the baseline intensity where both local and global data were recorded (36.7 R*/rod/s on average), the thresholds of the ideal observer were 7.65×10^{-3}, 7.61×10^{-3} and 7.46×10^{-5} R*/rod for local increments, local decrements, and for global stimuli (identical for increments and decrements) respectively. These values are 1.90, 1.74 and 2.78 log units lower than the respective human data values.

For the ideal observer, the difference between local and global thresholds remains fixed at all times. This is not the case for human observers, where a steeper increase in global thresholds reflects the limits of spatial summation, a factor that was not included in the ideal observer model. The ideal observer simulations produce asymmetries between increment and decrement thresholds only at the very lowest background intensities. The asymmetry then quickly becomes miniscule, decreasing to only 0.5% by the brightest background intensities used in the experiment. When the total amount of R* is considered, processing of global thresholds is exceedingly more efficient for global than for local stimuli (panel A of *Figure 10*). The opposite is true when examining the thresholds in R* per rod (panel B of *Figure 10*).

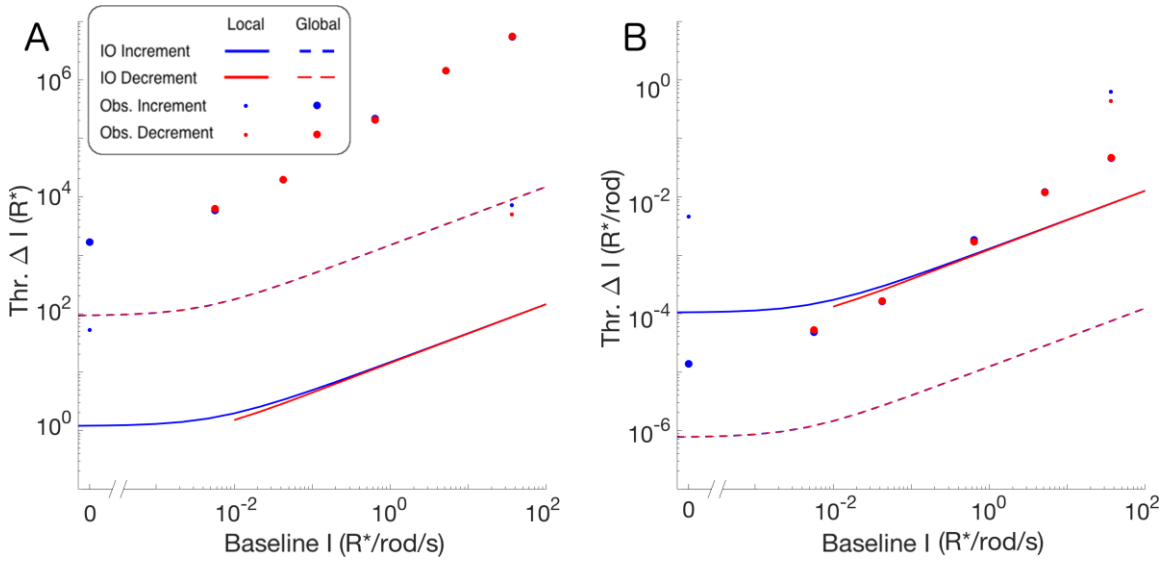

Figure 10. Ideal observer performance compared with experimental data, averaged across three participants (1, 2 & 3). (A) 75% detection threshold values in total retinal R* plotted against baseline light intensity. (B) 75% detection threshold values in R* per rod. The data point for local increment detection threshold with zero baseline light includes an outlier. With respect to the units in plot (B), the threshold of this participant was 0.0093 (*SD* = 0.0008) R*/rod. The mean threshold of the other participants in this condition was 0.0022 (*SD* = 0.0006) R*/rod.

Discussion

The current study examined increment and decrement detection thresholds with local and global stimuli. A significant asymmetry was observed between local increment and decrement thresholds. With global stimuli, increment and decrement thresholds show highly consistent symmetry across all participants and all background light levels.

Asymmetry with local but not with global thresholds

The higher sensitivity for decrements than increments in human visual processing is a highly ubiquitous finding (Lu & Sperling, 2012). Expectedly, when the experimental conditions of the current study were similar to those of Short (1966) and Patel & Jones (1968), and the stimulus was a small spot, the asymmetry was found for all three participants. Measurements with a local stimulus were not the main interest of the current study, and were restricted to one background intensity only. Our stimulus apparatus lacked the dynamic range required for higher background levels, and the difficulty of the decrement detection task complicated lower background levels. With one participant however, both a 40% higher background light level, and a roughly one log-unit lower background light level were also used to measure sensitivity. In this limited dataset, the asymmetry seemed to decrease with an increased background light level, also comporting with the findings of Short (1966) and Patel & Jones (1968), but not those of Herrick (1956). A tempting conclusion from this would be to relate the asymmetry to pathways initiated from rods. As intensities increase further into the photopic range, rods are responsible for a relatively smaller proportion of signal processing, despite their outstanding capability to avoid absolute saturation by adapting (Tikidji-Hamburyan et al., 2017). Nonetheless, complete symmetry is not observed under photopic conditions either (Kremkow et al., 2014). Whether this asymmetry can be ascribed to the rod bipolar pathway not becoming fully saturated, or to another source in the cone pathways, remains unresolved.

When the stimulus covered the full visual field, the sensitivity for increment and decrement stimuli remained equal for all participants, for all baseline light levels. The

symmetry was nearly perfect. Global increment thresholds were only 0.7% higher than decrement thresholds, contrasted with 44.0% (*SD* = 5.9) for the local threshold comparison. In the peripheral vision, a complete lack of asymmetry is a very rare finding that contradicts most of the literature on the subject.

The absolute detection threshold of human vision is very low

When considering the vast number of rod cells, the absolute thresholds appear very low. The local stimulus covers approximately 11470 rod cells. It follows that at the detection threshold, only an average of 0.00224 (*SD* = 0.00065) R* per rod take place. This reaffirms Hecht, Schlaer and Pirenne's (1942) assertion, that it is very unlikely that two photons in any single rod are needed in one rod to produce a visual phenomenon. With fullfield stimuli, the small number of required R* per rod is even more remarkable. As each retina contains roughly 120 million rods (Cage & Baars, 2018), only 0.0000138 (*SD* = 0.0000032) R* per rod is enough for the 75% threshold.

These detection thresholds come close, but not quite to the level of classic psychophysics experiments. In the local detection task, only 25.7 (*SD* = 7.4) photoisomerizations sufficed for a 75% detection level in the dark, when participant 3 (106.1 R*, *SD* = 9.1) is discarded as an outlier. This number is considerably higher than *ca*. 10, found by Hecht, Schlaer and Pirenne (1942). The controls used in the current study deviated slightly from the classic experiment: eccentricity was 15% lower, and the stimulus duration was 10 times longer. More importantly, the stimulus used in the current study was seven times larger in diameter, which might exceed Riccò's area of complete spatial summation (Barlow, 1958). With fullfield thresholds the total number of R* increases over 60-fold, with the mean of 1660, and a standard deviation of 380 R*.

Ideal observer model reveals that Poisson variation is not enough to explain the asymmetry

Sensitivity can be infinite only in the complete absence of noise. Visual sensitivity of detection and discrimination are ultimately rendered finite by at least the Poisson fluctuations that act as a source of noise. A detection task can be conceptualized as a task to correctly classify samples drawn from two Poisson distributions; the baseline

distribution, and the stimulus distribution. The mean of the increment distribution is higher than that of the baseline distribution, and the mean of the decrement distribution is lower than that of the baseline distribution. For any Poisson distribution, variance is equal to the mean of the distribution. Compared to the baseline distribution, a distribution with an increment stimulus will always be wider than a distribution with a decrement stimulus. Therefore, the overlap between the baseline distribution and the increment distribution is larger than the overlap between the baseline distribution, and the distribution of a decrement stimulus of equal magnitude. This leads to potentially better decrement detectability. At very low light levels, quantum noise can probably cause some degree of asymmetry between increment and decrement detection thresholds (Cohn, 1974). With higher light levels, the difference between the variances of the increment distribution and the decrement distribution does increase, but in relative terms it becomes more negligible, as the variances themselves increase proportionally with the mean. In the current study, local stimulus detection thresholds were asymmetric at light levels where detectable stimuli are in the range of thousands of R*.

The possible roles of Poisson variation and dark noise in different backgrounds were more formally studied with an ideal observer model. Poisson variation and a dark noise rate of 0.0038 events per second acted as the only constraints on the model. Both factors pose completely inescapable limitations on absolute sensitivity of any real or ideal observer. When plotted against baseline intensities, all increment thresholds become asymptotic to the limit given by the dark noise rate (*Figure 10*). At this limit, photon absorptions are too sparse to be discriminated from neural noise at a 75% performance level. The local detection thresholds of this ideal observer are higher for increments only at the very lowest baseline intensities. With baseline intensities corresponding to those used in the current study, the asymmetry between increments and decrements is only 0.5%. Based on this performance it is obvious that the role of Poisson variation is negligible, and cannot explain the observed 44% asymmetry.

The ideal observer model only includes two basic preneural factors, one at the level of photons and one at the level of photopigments. As intended, this model is optimized for minimizing the thresholds. In reality, the functional organization of the retina may not have been selected for its ability to detect increments and decrements at

the threshold level. The mammalian visual system aims to generate a constant stream of visual sensation, with emphasis also on spatial resolution and temporal resolution. Increasing performance in either of these comes with a physiological trade-off in sensitivity (Koskela, 2020). In general, large photoreceptors and receptive fields are required for sensitivity. Their size has to remain moderate, however, due the inverse correlation between the size of photoreceptors and spatial and temporal resolution, as well as the inverse correlation between the size of RGCs and spatial resolution. The sacrificed sensitivity that results from the constraints of photoreceptor and retinal ganglion cell size could be included in a more realistic ideal observer model.

In addition to cellular-level properties of rod photoreceptors and RGCs, several system level retinal mechanisms are also required for a more realistic model. The retina features pooling and thresholding mechanisms that are considered to serve important purposes in minimizing this noise and maximizing the signal (Pahlberg & Sampath, 2011). For example, linear filtering in rod photoreceptors and a nonlinear threshold in rod bipolar cells reduce both continuous and discrete intrinsic noise. This enables convergence without pooling of intrinsic noise from photoreceptors that do not detect a stimulus. Differences between ON and OFF pathways, such as the vast difference in the number of ON and OFF RGCs, may also play a role in shaping the detection thresholds. Incorporating such factors into the ideal observer model would enable more accurate prediction of increment and decrement detection. Lastly, observers are also limited by noise caused by spontaneous activity later in the visual pathway, also not included in the ideal observer model.

Thresholds follow a hybrid of Weber's and de Vries-Rose laws

According to Weber's law, the ratio between detection thresholds and baseline intensities remains constant. When a threshold that follows Weber's law is plotted a log-log scale, the slope equals one. In most experimental settings where the stimulus is small and brief, detection thresholds at lower baseline intensities follow de Vries-Rose law (Brown & Rudd, 1998). This law states that the detection threshold increases proportionally to the square root of an increase in baseline intensity. As a result, the slope on a log-log scale is equal to 0.5. For light increments and decrements, the light level

domains of de Vries-Rose law and Weber's law remain poorly defined. Generally, the de Vries-Rose range applies to scotopic intensities, whereas a transition to Weber's range takes place where photopic range starts (Rovamo, Mustonen, & Näsänen, 1995). Transition from de Vries-Rose law to Weber's law has been considered to reflect switching from rod mediated vision to cone mediated, although under certain conditions, the transition seems too abrupt to be fully ascribed to this explanation (Rovamo et al., 1995). Transition at this point holds for foveal stimuli. With parafoveal and peripheral stimuli, de Vries–Rose law can extend into the photopic range (Bierings, de Boer, & Jansonius, 2018; Reeves, Wu, & Schirillo, 1998) With larger stimuli however, sensitivity begins to follow Weber's law at lower intensities (Barlow, 1957), which is in line with the current results.

The current study on global stimuli reveals consistently threshold versus intensity –curves that deviate from earlier findings with other stimuli. At the lowest intensities, thresholds followed a log-log slope of 0.57 for increments and 0.54 for decrements, thus almost obeying the de Vries-Rose law. At mesopic intensities, the curves are at their steepest. Increment thresholds have a slope of 0.91 and decrement stimuli have a slope of 0.96, roughly changing according to Weber's law. Finally, at photopic levels, the slopes return to the middle of what the two laws would predict (log-log slopes of 0.73 and 0.72 for increments and decrements, respectively). This slight re-flattening of the curve is surprising and not predicted by previous literature. With no data at higher baseline intensities, the extent of this flatter section, let alone its explanation, will remain unknown.

Speculations for the asymmetric detection thresholds with local stimuli

What then, if not the Poisson fluctuation, might account for the asymmetry between increment and decrement thresholds? Firstly, ON RGCs respond not only to increments, but also provide a graded response to decrements (Chichilnisky & Kalmar, 2002). OFF RGCs do not have this feature, and remain largely unresponsive to increments. Another factor might be related to the morphology of the ON and OFF RGCs, more specifically the differences in their dendritic field diameters. Dacey and Petersen (1992) found ON RGCs to be 30-50% larger in dendritic field diameter than

their OFF RGC counterparts. This held true across the studied eccentricity range of 7-50 degrees from the fovea. The receptive field of OFF RGCs is also smaller, as evidenced by their tuning to Gabor patches with higher spatial frequency (Tyler, Chan, & Liu, 1992). Owing to this fact, the OFF RGCs form a denser mosaic. This morphological asymmetry, and the almost two-fold difference in cell quantity, has been proposed to be a structural adaptation to natural scenes involving more decrements than increments (Ratliff et al., 2010).

Since the OFF RGCs are more numerous and yet have the same synaptic density as that of ON RGCs, the synaptic density per retinal area is higher for the OFF pathway (Ratliff et al., 2010). Conceptually, an array of OFF RGCs can process more information than an array of ON RGCs covering an equal area. It may be chiefly for this reason that the sensitivity for decrements is consistently higher with local stimuli.

This does not, however, explain the symmetric thresholds in fullfield detection. This finding appears particularly surprising, considering the ubiquity of the asymmetry with spatially restricted stimuli (Lu & Sperling, 2012). It also appears curious in light of recent *in vivo* recordings from primate visual cortex. In corticocortical layers 2 and 3 of the primary visual cortex, neurons responding primarily to decrements vastly outnumber those coding for increments (Yeh et al., 2009). However, when the size of grating stimuli was decreased, the dominance diminished (Jansen et al., 2019). The same effect was produced by increasing the grating frequency of the stimulus. In this case, the asymmetry was not found when a smaller portion of the visual field is stimulated, i.e. when the stimuli are perceived as more distant. Although the asymmetry found in the current study was also dependent on the stimulus size, it was also in the opposite direction, and hence in contradiction with the results of Jansen et al. (2019).

When the array of RGCs is sufficiently large, resolving of information may be limited by other factors than asymmetries in RGC properties or organization. Limitations may also arise from spatial integration over all RGCs. It has been suggested that Riccò's area in different eccentricities is determined by the amount of underlying RGCs – perfect spatial integration holds for up to roughly 14 RGCs (Kwon & Liu, 2019). Piper's square root summation rules, that apply for larger areas up to 20°, have been attributed to aggregated noise that is intrinsic to long-range connections (Meese, 2010). As stimulus

size increases to the full visual field, sensitivity has been proposed to vary inversely proportionally with the cube root of the area. (Ruseckaite, Lamb, Pianta, & Cameron, 2011). According to the authors, this log-log slope of -1/3 likely reflects probability summation across retinal ganglion cells, the idea that a stimulus is detected when a threshold level is reached in sufficiently many independent receptive fields. Probability summation has received criticism with both conceptual and empirical basis (Laming, 2013). It seems likely that spatial summation in the periphery is better described by multiple mechanisms of cortical pooling (Pan & Swanson, 2006). In either case, integrating information over a large number of RGCs can potentially set a sensitivity limit that overrides the advantage OFF RGCs have in resolving more local information. Unfortunately, however, pooling mechanisms have not been studied with decrements, as widely as they have with increments.

Practical limitations

Certain confounding variables may limit the interpretability of the data. A target located 18° from the fovea is distant enough to cause some degree of spatial uncertainty. Even if a participant can pay close covert attention to the anticipated target location, his or her prediction can be off by enough to cause a decrease in sensitivity (Cohn & Lasley, 1974). Fading of a peripheral target, also known as Troxler fading, is a phenomenon that could also lower the sensitivity for local stimuli. Troxler fading can be explained by shortcomings in the magnitude of microsaccades, the miniature eye movements assumed to suppress neural adaptation. At certain eccentricities, microsaccades are too small in relation to large receptive fields, and the small spot stimulus will keep falling on the same receptive field (Martinez-Conde, Macknik, & Hubel, 2004). Instructed fixation on one spot has been found to further decrease the magnitude of microsaccades (Winterson & Collewun, 1976).

Conclusion

As a conclusion, the well-established asymmetry between increment and decrement detection thresholds was successfully replicated with local stimuli. As evidenced by the ideal observer analysis, Poisson fluctuations and dark noise are not the

primary sources of this asymmetry. An unusual symmetry between the increment and decrement thresholds was found when stimuli were not spatially restricted.

Acknowledgements

I want to express my deepest gratitude to my supervisor, Dr. Markku Kilpeläinen, for his invaluable guidance and encouragement. This project would not have been completed without his persistent help and great advice. Thank you to Prof. Petri Ala-Laurila for his wisdom and inspiration as the leader and the second supervisor of this project, and to Prof. Kristian Donner for sharing his vast knowledge. I am indebted to Anton Laihi for his countless ways of helping, including but not limited to: collecting a part of the data used for the thesis, thoroughly orienting me with the methods from data collection to analysis, and by being available to help with many hurdles throughout. I wish to send my special regards to Johan Westö, who provided the ideal observer model for this thesis, and to the rest of the lab members, from whom I have gained much information that facilitated the realization of this thesis.

References

Aguilar, M., & Stiles, W. S. (1971). Saturation of the rod mechanism of the retina at high levels of stimulation. *Optica Acta*. http://doi.org/10.1080/09500347109696914

Ahmad, K. M., Klug, K., Herr, S., Sterling, P., & Schein, S. (2003). Cell density ratios in a foveal patch in macaque retina. *Visual Neuroscience*. http://doi.org/10.1017/S0952523803202091

Ala-Laurila, P., & Rieke, F. (2014). Coincidence detection of single-photon responses in the inner retina at the sensitivity limit of vision. *Current Biology*, *24*(24), 2888–2898. http://doi.org/10.1016/j.cub.2014.10.028

Barlow, H. B. (1957). Increment thresholds at low intensities considered as signal/noise discriminations. *The Journal of Physiology*, *136*(3), 469–488. http://doi.org/10.1113/jphysiol.1957.sp005774

Barlow, H. B. (1958). Temporal and spatial summation in human vision at different background intensities. *The Journal of Physiology*, *141*, 337–350. http://doi.org/10.1113/jphysiol.1958.sp005978

Barlow, H. B. (1977). Retinal and central factors in human vision limited by noise. In Barlow, H. B. & Fatt, P. (Eds), *Vertebrate photoreception* (pp. 337-358). London: Academic Press.

Baylor, D. A., Matthews, G., & Yau, K. W. (1980). Two components of electrical dark noise in toad retinal rod outer segments. *The Journal of Physiology*, *309*, 591–621.

Benardete, E., & Kaplan, E. (1999). The dynamics of primate retinal ganglion cells. *Progress in Brain Research*, *16*, 355–368. http://doi.org/10.1016/S0079-6123(01)34003-7

Bierings, R. A. J. M., de Boer, M. H., & Jansonius, N. M. (2018). Visual performance as a function of luminance in glaucoma: The de vries-rose, weber's, and ferry-porter's law. *Investigative Ophthalmology and Visual Science*, *59*(8), 3416–3423. http://doi.org/10.1167/iovs.17-22497

Blackwell, H. R. (1946). Contrast thresholds of the human eye. *Journal of the Optical Society of America*, *36*(11), 624–643. http://doi.org/10.1364/JOSA.40.000825

Bowen, R. W., Pokorny, J., & Smith, V. C. (1989). Sawtooth contrast sensitivity:

Decrements have the edge. *Vision Research*, *29*(11), 1501–1509. http://doi.org/10.1016/0042-6989(89)90134-X

Brown, L. G., & Rudd, M. E. (1998). Evidence for a noise gain control mechanism in human vision. *Vision Research*, *38*(13), 1925–1933. http://doi.org/10.1016/S0042-6989(97)00400-8

Buchner, A., & Baumgartner, N. (2007). Text - Background polarity affects performance irrespective of ambient illumination and colour contrast. *Ergonomics*, *50*(7), 1036–1063. http://doi.org/10.1080/00140130701306413

Chichilnisky, E. J., & Kalmar, R. S. (2002). Functional Asymmetries in ON and OFF Ganglion Cells of Primate Retina. *Journal of Neuroscience*, *22*(7), 2737–2747. http://doi.org/10.1523/jneurosci.22-07-02737.2002

Cohn, T.E. (1974). A new hypothesis to explain why the increment threshold exceeds the decrement threshold. *Vision Res.*, *14*(11), 1277-9. http://doi.org/10.1016/0042-6989(74)90228-4.

Cohn, T. E., & Lasley, D. J. (1974). Detectability of a Luminance Increment: Effect of Spatial Uncertainty. *J Opt Soc Am*, *64*(12), 1715–1719. http://doi.org/10.1364/JOSA.64.001715

Cooper, E. A., & Norcia, A. M. (2015). Predicting Cortical Dark/Bright Asymmetries from Natural Image Statistics and Early Visual Transforms. *PLoS Computational Biology*, *11*(5), 1–25. http://doi.org/10.1371/journal.pcbi.1004268

Dacey, D. M., & Petersen, M. R. (1992). Dendritic field size and morphology of midget and parasol ganglion cells of the human retina. *Proceedings of the National Academy of Sciences of the United States of America*, *89*(20), 9666–9670. http://doi.org/10.1073/pnas.89.20.9666

de Vries, H. L. (1943). The quantum character of light and its bearing upon threshold of vision, the differential sensitivity and visual acuity of the eye. *Physica*, *10*, 553–564. http://doi.org/10.1016/S0031-8914(43)90575-0

Donner, K. (1992). Noise and the absolute thresholds of cone and rod vision. *Vision Research*, *32*(5), 853–866. http://doi.org/10.1016/0042-6989(92)90028-H

Donner, K., Copenhagen, D. R., & Reuter, T. (1990). Weber and noise adaptation in the retina of the toad Bufo marinus. *Journal of General Physiology*, *95*(4), 733–753.

http://doi.org/10.1085/jgp.95.4.733

Elandt-Johnson, R. C., & Johnson, N. L. (1980). *Survival models and data analysis* (1st ed.). John Wiley & Sons.

Field, G. D., & Sampath, A. P. (2017). Behavioural and physiological limits to vision in mammals. *Philosophical Transactions of the Royal Society B: Biological Sciences*, *372*(1717). http://doi.org/10.1098/rstb.2016.0072

Field, G. D., Sampath, A. P., & Rieke, F. (2005). RETINAL PROCESSING NEAR ABSOLUTE THRESHOLD: From Behavior to Mechanism. *Annual Review of Physiology*, *67*(1), 491–514. http://doi.org/10.1146/annurev.physiol.67.031103.151256

Gage, N. M., & Baars, B. J. (2018). The Art of Seeing. In *Fundamentals of cognitive neuroscience: A beginner's guide* (2nd ed., pp. 99-141). Academic Press.

Gjorgjieva, J., Sompolinsky, H., & Meister, M. (2014). Benefits of pathway splitting in sensory coding. *Journal of Neuroscience*, *34*, 12127–12144. http://doi.org/10.1523/JNEUROSCI.1032-14.2014

Goodchild, A. K., Ghosh, K. K., & Martin, P. R. (1996). Comparison of photoreceptor spatial density and ganglion cell morphology in the retina of human, macaque monkey, cat, and the marmoset Callithrix jacchus. *Journal of Comparative Neurology*, *366*, 55–75. http://doi.org/10.1002/(SICI)1096-9861(19960226)366:1<55::AID-CNE5>3.0.CO;2-J

Grimes, W. N., Baudin, J., Azevedo, A., & Rieke, F. (2018). Rod signaling in primate retina: Range, routing and kinetics. *BioRxiv*, *7*, 1–21. http://doi.org/10.1101/352419

Hall, M. I., Kamilar, J. M., & Christopher Kirk, E. (2012). Eye shape and the nocturnal bottleneck of mammals. *Proceedings of the Royal Society B: Biological Sciences*, *279*(1749), 4962–4968. http://doi.org/10.1098/rspb.2012.2258

Harmening, W. M. (2017). Kontrastempfindlichkeit und Sehschärfe bei Tieren. *Ophthalmologe*, *114*(11), 986–996. http://doi.org/10.1007/s00347-017-0561-4

Hecht, S., Shlaer, S., & Pirenne, M. H. (1942). Energy, Quanta and Vision. *The Journal of General Physiology*, *25*(6), 819–840. http://doi.org/10.1085/jgp.25.6.819

Herrick, R. M. (1956). Foveal luminance discrimination as a function of the duration of the decrement or increment in luminance. *Journal of Comparative and Physiological Psychology, 49*(5), 437–443. https://doi.org/10.1037/h0046317

Jansen, M., Jin, J., Li, X., Lashgari, R., Kremkow, J., Bereshpolova, Y., … Alonso, J. M. (2019). Cortical Balance between on and off Visual Responses Is Modulated by the Spatial Properties of the Visual Stimulus. *Cerebral Cortex*, *29*(1), 336–355. http://doi.org/10.1093/cercor/bhy221

Jiang, Y., Purushothaman, G., & Casagrande, V. A. (2015). The Functional Asymmetry of ON and OFF Channels in the Perception of Contrast. *Journal of Neurophysiology*, jn.00560.2015. http://doi.org/10.1152/jn.00560.2015

Karklin, Y., & Simoncelli, E. P. (2011). Efficient coding of natural images with a population of noisy Linear-Nonlinear neurons. *Efficient Coding of Natural Images with a Population of Noisy Linear-Nonlinear Neurons*, *24*, 999–1007.

Kingdom, F. A., & Prins, N. (2016). *Psychophysics: A practical introduction* (2nd ed.). Academic Press.

Kolb, H. (1970). Organization of the outer plexiform layer of the primate retina: electron microscopy of Golgi-impregnated cells. *Philosophical Transactions of the Royal Society of London. Series B, Biological Sciences*, *258*, 261–283. http://doi.org/10.1098/rstb.1970.0036

Komban, S. J., Alonso, J. M., & Zaidi, Q. (2011). Darks are processed faster than lights. *Journal of Neuroscience*, *31*(23), 8654–8658. http://doi.org/10.1523/JNEUROSCI.0504-11.2011

Komban, S. J., Kremkow, J., Jin, J., Wang, Y., Lashgari, R., Li, X., … Alonso, J. M. (2014). Neuronal and perceptual differences in the temporal processing of darks and lights. *Neuron*, *82*(1), 223–234. http://doi.org/10.1016/j.neuron.2014.02.020

Koskela, S. (2020). *The limits of visual sensitivity and its circadian control.* (Doctoral dissertation). University of Helsinki, Helsinki, Finland. Helda Dissertations Publishing.

Koskela, S., Turunen, T., & Ala-Laurila, P. (2020). Mice Reach Higher Visual Sensitivity at Night by Using a More Efficient Behavioral Strategy. *Current Biology*, *30*(1), 42–53.e4. http://doi.org/10.1016/j.cub.2019.11.021

Kremers, J., Lee, B. B., Pokorny, J., & Smith, V. C. (1993). Responses of macaque ganglion cells and human observers to compound periodic waveforms. *Vision Research*, *33*(14), 1997–2011. http://doi.org/10.1016/0042-6989(93)90023-P

Kremkow, J., Jin, J., Komban, S. J., Wang, Y., Lashgari, R., Li, X., … Alonso, J. (2014). Neuronal nonlinearity explains greater visual spatial resolution for darks than lights. *PNAS*, *111*(8), 3170–3175. http://doi.org/10.1073/pnas.1310442111

Kwon, M. Y., & Liu, R. (2019). Linkage between retinal ganglion cell density and the nonuniform spatial integration across the visual field. *Proceedings of the National Academy of Sciences of the United States of America*, *116*(9), 3827–3836. http://doi.org/10.1073/pnas.1817076116

Laming, D. (2013). Probability summation — a critique, *30*(3), 300–315.

Lu, Z. L., & Sperling, G. (2012). Black-white asymmetry in visual perception. *Journal of Vision*, *12*(10), 1–21. http://doi.org/10.1167/12.10.8

Margolis, D. J., & Detwiler, P. B. (2007). Different mechanisms generate maintained activity in ON and OFF retinal ganglion cells. *Journal of Neuroscience*, *27*(22), 5994–6005. http://doi.org/10.1523/JNEUROSCI.0130-07.2007

Martinez-Conde, S., Macknik, S. L., & Hubel, D. H. (2004). The role of fixational eye movements in visual perception. *Nature Reviews Neuroscience*. http://doi.org/10.1038/nrn1348

Mazade, R., Jin, J., Pons, C., & Alonso, J. M. (2019). Functional Specialization of ON and OFF Cortical Pathways for Global-Slow and Local-Fast Vision. *Cell Reports*, *27*(10), 2881–2894. http://doi.org/10.1016/j.celrep.2019.05.007

Meese, T. S. (2010). Spatially extensive summation of contrast energy is revealed by contrast detection of micro-pattern textures. *Journal of Vision*, *10*(8), 1–21. http://doi.org/10.1167/10.8.14

Murphy, G., Rieke, F. Signals and noise in an inhibitory interneuron diverge to control activity in nearby retinal ganglion cells. *Nat Neurosci*, *11*, 318–326 (2008). https://doi.org/10.1038/nn2045

Østerberg, G. (1935). Topography of the layer of rods and cones in the human retina. *Acta Ophthalmologica*, *13*, 1-103.

Pahlberg, J., & Sampath, A. P. (2011). Visual threshold is set by linear and nonlinear

mechanisms in the retina that mitigate noise: How neural circuits in the retina improve the signal-to-noise ratio of the single-photon response. *BioEssays*. http://doi.org/10.1002/bies.201100014

Pan, F., & Swanson, W. H. (2006). A cortical pooling model of spatial summation for perimetric stimuli. *Journal of Vision*, *6*(11), 1159–1171. http://doi.org/10.1167/6.11.2

Pandarinath, C., Victor, J. D., & Nirenberg, S. (2010). Symmetry Breakdown in the ON and OFF Pathways of the Retina at Night: Functional Implications. *Journal of Neuroscience*, *30*(30), 10006–14. http://doi.org/10.1523/JNEUROSCI.5616-09.2010

Patel, A. S., & Jones, R. W. (1968). Increment and decrement visual thresholds .*Journal of the Optical Society of America*, *58,* 696 –699.

Patel, A. S., & Jones, R. W. (1968). Increment and Decrement Visual Thresholds. *Journal of the Optical Society of America*, *58*(5), 696–699. http://doi.org/10.1364/JOSA.58.000696

Piper, H. (1903). Über Dunkeladaptation. *Zeitschrift für Psychologie und Physiologie der Sinnesorgane, 31*, 161-214.

Pons, C., Mazade, R., Jin, J., Dul, M. W., Zaidi, Q., & Alonso, J.-M. (2017). Neuronal mechanisms underlying differences in spatial resolution between darks and lights in human vision. *Journal of Vision*, *17*(14), 5. http://doi.org/10.1167/17.14.5

Puolakka M., Cengiz C., Luo W., Halonen L. (2012). Implementation of CIE 191 Mesopic Photometry – Ongoing and Future Actions. *Proceedings CIE 2012 Lighting Quality and Energy Efficiency*. Hangzhou, China, Sep 19–21 2012, 64–70.

Ratliff, C. P., Borghuis, B. G., Kao, Y. H., Sterling, P., & Balasubramanian, V. (2010). Retina is structured to process an excess of darkness in natural scenes. *Proceedings of the National Academy of Sciences of the United States of America*, *107*(40), 17368–17373. http://doi.org/10.1073/pnas.1005846107

Ravi, S., Ahn, D., Greschner, M., Chichilnisky, E. J., & Field, G. D. (2018). Pathway-Specific Asymmetries between ON and OFF Visual Signals. *The Journal of Neuroscience*, *38*(45), 9728–9740. http://doi.org/10.1523/JNEUROSCI.2008-18.2018

Raviola, E., & Gilula, N. (1973). Gap junctions between photoreceptor cells in the

vertebrate retina. *PNAS*. http://doi.org/10.1073/pnas.70.6.1677

Reeves, A., Wu, S., & Schirillo, J. (1998). The effect of photon noise on the detection of white flashes. *Vision Research*, *38*(5), 691–703. http://doi.org/10.1016/S0042-6989(97)00201-0

Rose, A. (1948). The sensitivity performance of the human eye on an absolute scale. *Journal of the Optical Society of America*, *38*, 196–208. http://doi.org/10.1364/JOSA.38.000196

Rovamo, J., Mustonen, J., & Näsänen, R. (1995). Neural modulation transfer function of the human visual system at various eccentricities. *Vision Research*, *35*(6), 767–774. http://doi.org/10.1016/0042-6989(94)00171-H

Ruseckaite, R., Lamb, T. D., Pianta, M. J., & Cameron, A. M. (2011). Human scotopic dark adaptation: Comparison of recoveries of psychophysical threshold and ERG b-wave sensitivity. *Journal of Vision*, *11*(8), 1–16. http://doi.org/10.1167/11.8.1

Sakitt, B. (1972). Counting every quantum. *The Journal of Physiology*, *223*(1), 131–150. http://doi.org/10.1113/jphysiol.1972.sp009838

Schiller, P. H. (1992). The ON and OFF channels of the visual system. *Trends in Neurosciences*. http://doi.org/10.1016/0166-2236(92)90017-3

Shapley, R., & Enroth-Cugell, C. (1984). Visual Adaptation and Retinal Gain Controls. *Engineering Sciences*, *3*, 263–346.

Short, A. D. (1966). Decremental and incremental visual thresholds. *The Journal of Physiology*, *185*(3), 646–654. http://doi.org/10.1113/jphysiol.1966.sp008007

Soucy, E., Wang, Y., Nirenberg, S., Nathans, J., & Meister, M. (1998). A novel signaling pathway from rod photoreceptors to ganglion cells in mammalian retina. *Neuron*, *21*, 481–493. http://doi.org/10.1016/S0896-6273(00)80560-7

Stuart, A. & Ord, J.K. (1998). *Kendall's Advanced Theory of Statistics: Distribution Theory* (6th ed.), Oxford University Press, New York.

Takeshita, D., Smeds, L., & Ala-Laurila, P. (2017). Processing of single-photon responses in the mammalian on and off retinal pathways at the sensitivity limit of vision. *Philosophical Transactions of the Royal Society B: Biological Sciences*, *372*(1717), 1–10. http://doi.org/10.1098/rstb.2016.0073

Taylor, W. R., & Smith, R. G. (2004). Transmission of scotopic signals from the rod to

rod-bipolar cell in the mammalian retina. In *Vision Research*. http://doi.org/10.1016/j.visres.2004.07.043

Teich, M. C., & Saleh, B. E. A. (1982). Effects of random deletion and additive noise on bunched and antibunched photon-counting statistics. *Optics Letters*, *7*(8), 365. http://doi.org/10.1364/ol.7.000365

Thoreson, W. B., Babai, N., & Bartoletti, T. M. (2008). Feedback from Horizontal Cells to Rod Photoreceptors in Vertebrate Retina. *Journal of Neuroscience*. http://doi.org/10.1523/JNEUROSCI.0403-08.2008

Tiihonen, J. (2019). *Utilization of a single-photon gun to measure single-photon responses in retinal rods.* (Master's dissertation). Aalto University, Espoo, Finland.

Tikidji-Hamburyan, A., Reinhard, K., Storchi, R., Dietter, J., Seitter, H., Davis, K. E., … Münch, T. A. (2017). Rods progressively escape saturation to drive visual responses in daylight conditions. *Nature Communications*, *8*(1). http://doi.org/10.1038/s41467-017-01816-6

Turner, M. H., & Rieke, F. (2016). Synaptic Rectification Controls Nonlinear Spatial Integration of Natural Visual Inputs. *Neuron*, *90*(6), 1257–1271. http://doi.org/10.1016/j.neuron.2016.05.006

Tyler, C. W., Chan, H., & Liu, L. (1992). Different spatial tunings for ON and OFF pathway stimulation. *Ophthalmic and Physiological Optics*, *12*(2), 233–240. http://doi.org/10.1111/j.1475-1313.1992.tb00297.x

Van Der Velden, H. A. (1946). The number of quanta necessary for the perception of light of the human eye. *Ophthalmologica. Journal International d'ophtalmologie. International Journal of Ophthalmology. Zeitschrift Für Augenheilkunde*. http://doi.org/10.1159/000300352

Veilleux, C. C., & Kirk, E. C. (2014). Visual acuity in mammals: Effects of eye size and ecology. *Brain, Behavior and Evolution*, *83*(1), 43–53. http://doi.org/10.1159/000357830

Volgyi, B., Deans, M. R., Paul, D. L., & Bloomfield, S. A. (2004). Convergence and Segregation of the Multiple Rod Pathways in Mammalian Retina. *Journal of Neuroscience*, *24*(49), 11182–11192. http://doi.org/10.1523/JNEUROSCI.3096-04.2004

Wald, G. (2004). SELIG HECHT (1892–1947). *The Journal of General Physiology*, *32*, 1-16.

Wallach, H. (1948). Brightness constancy and the nature of achromatic colors. *Journal of Experimental Psychology*. http://doi.org/10.1037/h0053804

Werblin, F. S. (2010). Six different roles for crossover inhibition in the retina: Correcting the nonlinearities of synaptic transmission. *Visual Neuroscience*, *27*(1–2), 1–8. http://doi.org/10.1017/S0952523810000076

Winterson, B. J., & Collewun, H. (1976). Microsaccades during finely guided visuomotor tasks. *Vision Research*, *16*(12), 1387–1390. http://doi.org/10.1016/0042-6989(76)90156-5

Wu, C., Ivanova, E., Cui, J., Lu, Q., & Pan, Z. H. (2011). Action potential generation at an axon initial segment-like process in the axonless retinal AII amacrine cell. *Journal of Neuroscience*, *31*(41), 14654–14659. http://doi.org/10.1523/JNEUROSCI.1861-11.2011

Yeh, C. I., Xing, D., & Shapley, R. M. (2009). "Black" responses dominate macaque primary visual cortex V1. *Journal of Neuroscience*. http://doi.org/10.1523/JNEUROSCI.1991-09.2009

Zaghloul, K. a, Boahen, K., & Demb, J. B. (2003). Different circuits for ON and OFF retinal ganglion cells cause different contrast sensitivities. *The Journal of Neuroscience : The Official Journal of the Society for Neuroscience*, *23*(7), 2645–2654. http://doi.org/23/7/2645 [pii]

Zemon, V., Gordon, J., & Welch, J. (1988). Asymmetries in ON and OFF visual pathways of humans revealed using contrast-evoked cortical potentials. *Visual Neuroscience*, *1*(1), 145–150. http://doi.org/10.1017/S0952523800001085